Supplementary Information

Suppressing photo-oxidation of conjugated polymers and their blends with fullerenes through nickel chelates

Michael Salvador[1,5*], Nicola Gasparini[1], Jose Darío Perea[1], Sri Harish Paleti[2], Andreas Distler[2], Liana N. Inasaridze[3], Pavel A. Troshin[3], Larry Lüer[4], Hans-Joachim Egelhaaf[2], and Christoph Brabec[1]

[1]*Friedrich-Alexander University Erlangen-Nuremberg, Germany.*

[2]*ZAE Bayern, Erlangen, Germany.*

[3]*Skolkovo Institute of Science and Technology, Moscow, Russia.*

[4]*IMDEA, Nanoscience, Madrid, Spain.*

[5]*Instituto de Telecomunicações, Instituto Superior Técnico, Av. Rovisco Pais, P-1049-001 Lisboa, Portugal*

Correspondence to: michael.salvador@fau.de and christoph.brabec@fau.de

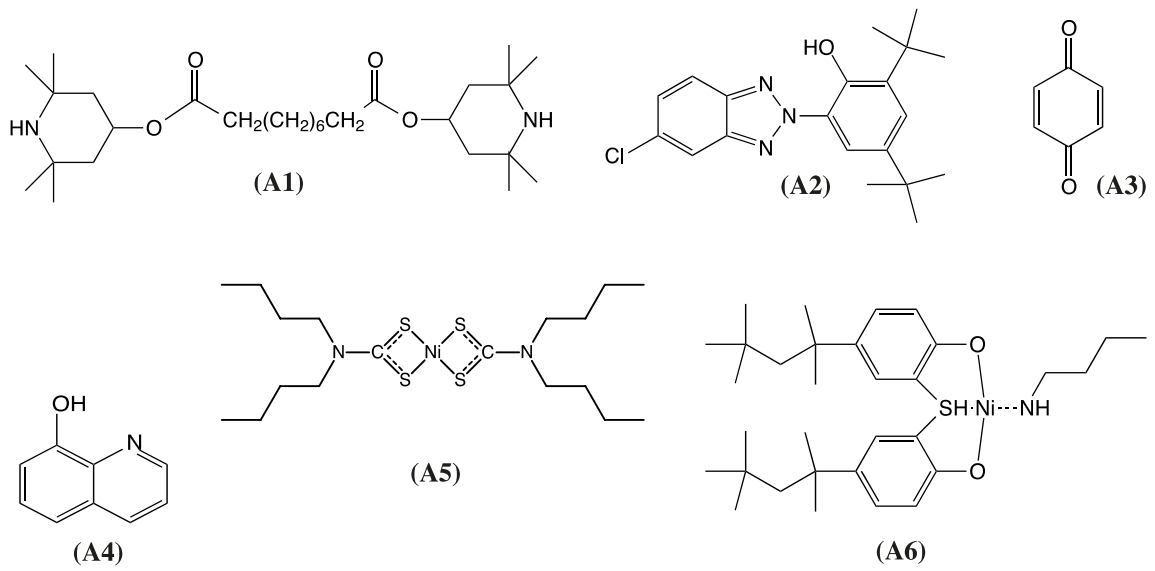

Figure S1. Molecular structures of antioxidants investigated for suppressing photo-oxidation of conjugated polymers (categorized by functionality). Hindered amine light stabilizer (HALS): (A1) Bis(2,2,6,6-tetramethyl-4-piperidyl) sebacate; hindered phenol: (A2) 2,4-Di-*tert*-butyl-6-(5-chloro-2*H*-benzotriazol-2-yl)phenol; electron donor: (A3) 1,4-Benzoquinone; metal chelating agent: (A4) 8-Hydroxyquinoline; Nickel chelates: (A5) Nickel(II) Dibutyldithiocarbamate, (A6) 2,2'-Thiobis(4-tert- octylphenolato)-n-butylamine nickel (II).

UV-VIS spectroscopy data of conjugated polymers P1 – P7 in the presence of antioxidants A1 – A6

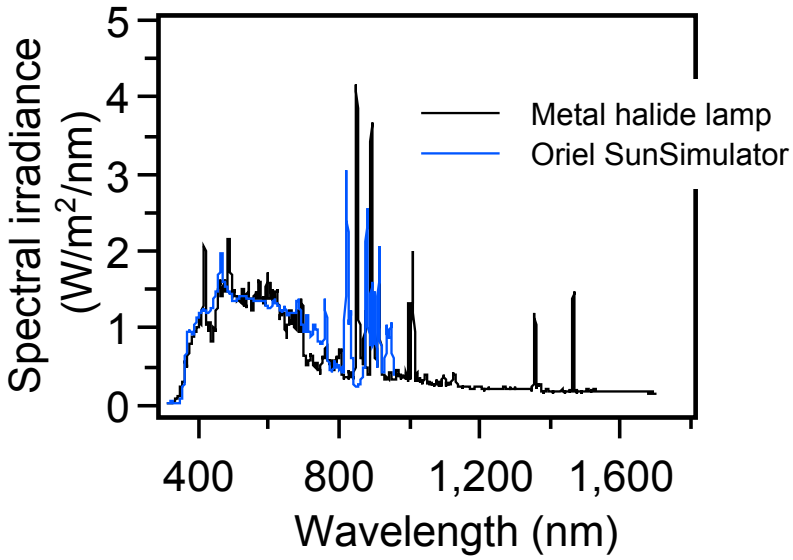

Figure S2. Spectral irradiance of solar simulators. Spectra of the solar simulator light used for photo-oxidizing polymer and polymer-fullerene blend films (*Metal halide lamp*, 4x150 W, 150R Solarlux Class B, Eye Lighting) and for characterizing solar cell devices (*Oriel SunSimulator*, Oriel Sol 1A, Newport).

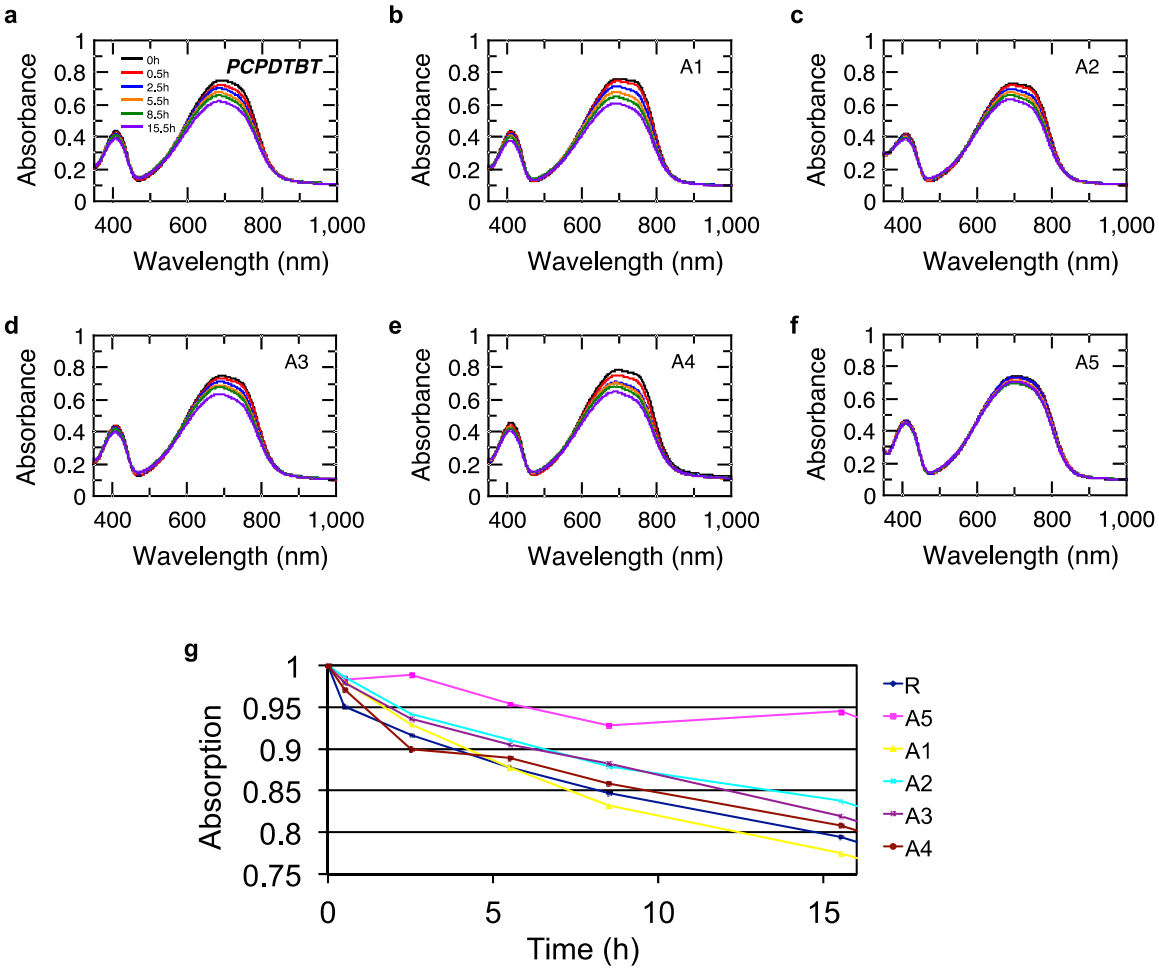

Figure S3. Reaction spectra of PCPDTBT films. a, neat PCPDTBT, **b – f**, PCPDTBT films containing 10wt% of the antioxidants A1 – A5 exposed to a solar simulator in air. **g**, Photooxidation kinetics of PCPDTBT films in the absence (R)/ presence of the additives A1 – A5.

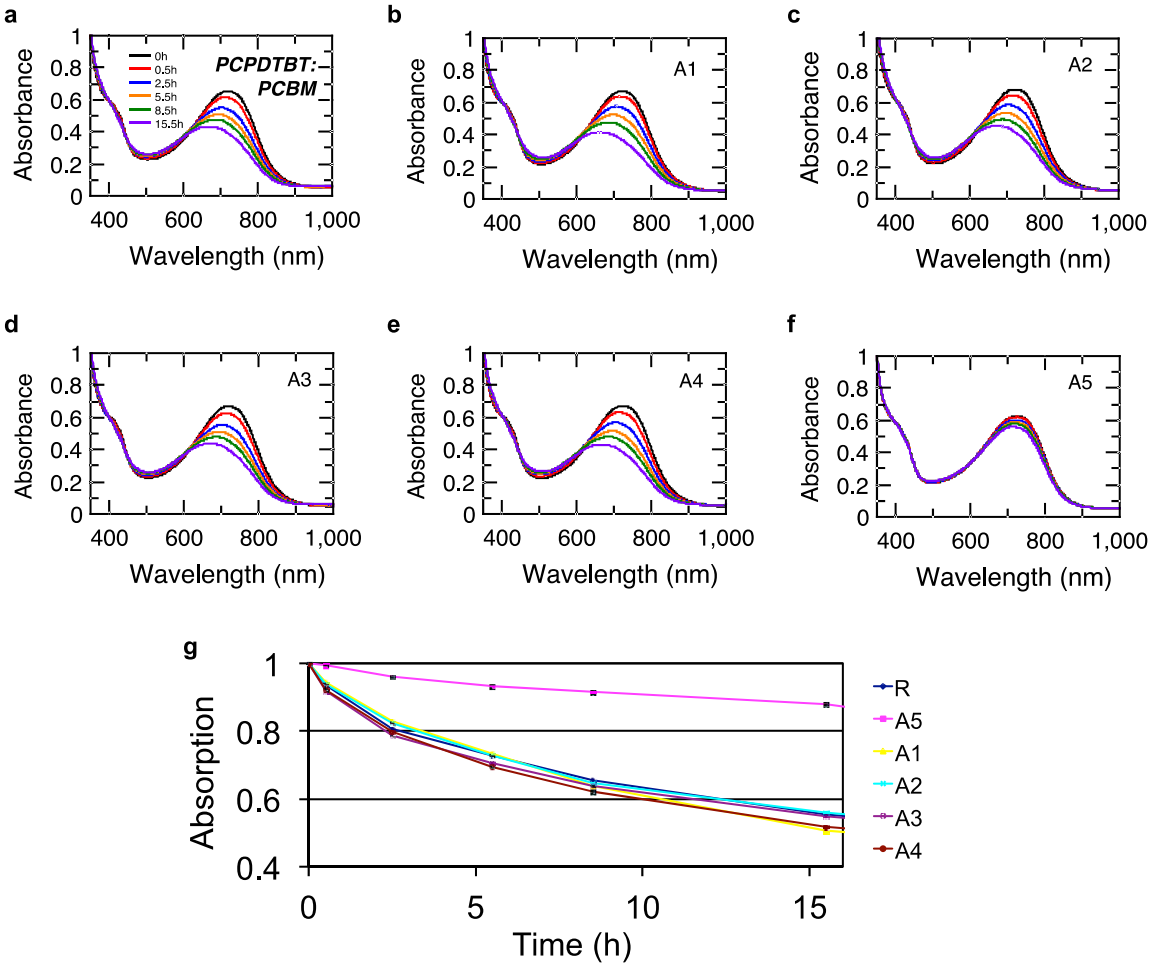

Figure S4. Reaction spectra of PCPDTBT:PC60BM blend films. a, PCPDTBT:PC60BM, **b – f**, PCPDTBT:PC60BM films containing 10wt% of the antioxidants A1 – A5 exposed to a solar simulator in air. **g**, Photooxidation kinetics of PCPDTBT:PC60BM films in the absence (R)/ presence of the additives A1 – A5.

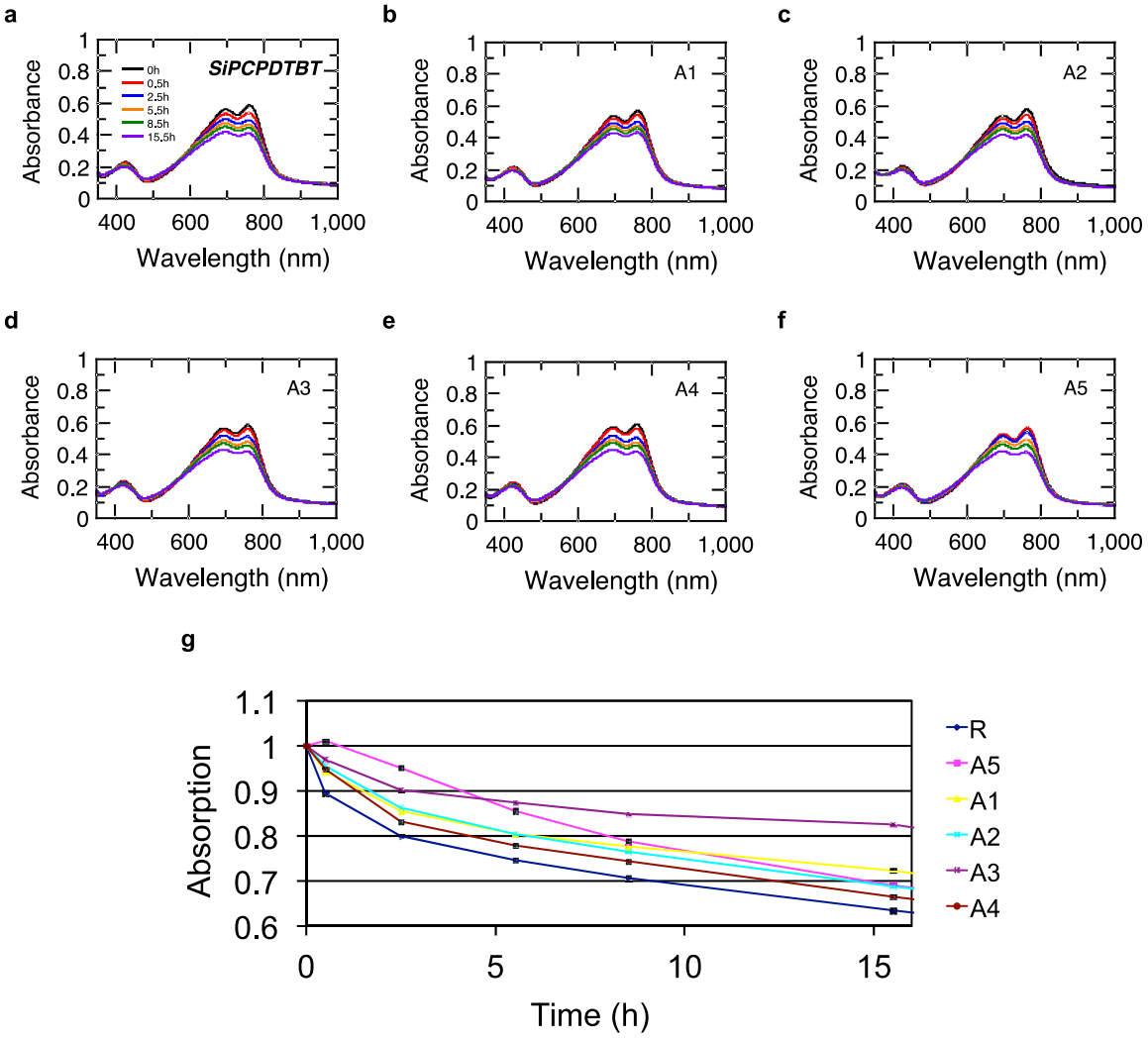

Figure S5. Reaction spectra of Si-PCPDTBT films. a, neat Si-PCPDTBT, **b – f**, PCPDTBT films containing 10wt% of the antioxidants A1 – A5 exposed to a solar simulator in air. **g**, Photooxidation kinetics of Si-PCPDTBT films in the absence (R)/ presence of the additives A1 – A5.

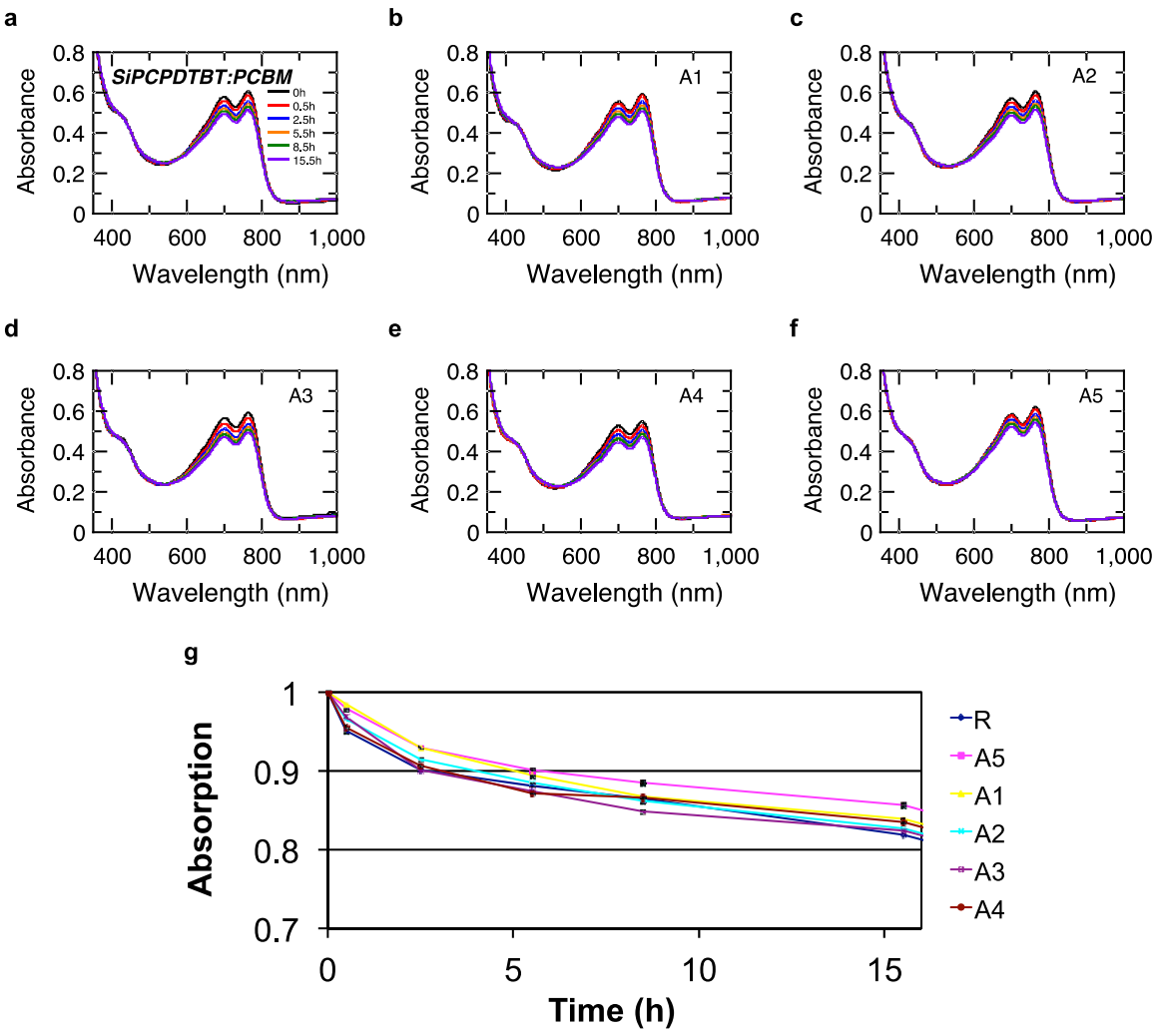

Figure S6. Reaction spectra of Si-PCPDTBT:PC60BM blend films. a, Si-PCPDTBT:PC60BM, **b – f**, Si-PCPDTBT:PC60BM films containing 10wt% of the antioxidants A1 – A5 exposed to a solar simulator in air. **g**, Photooxidation kinetics of Si-PCPDTBT:PC60BM films in the absence (R)/ presence of the additives A1 – A5.

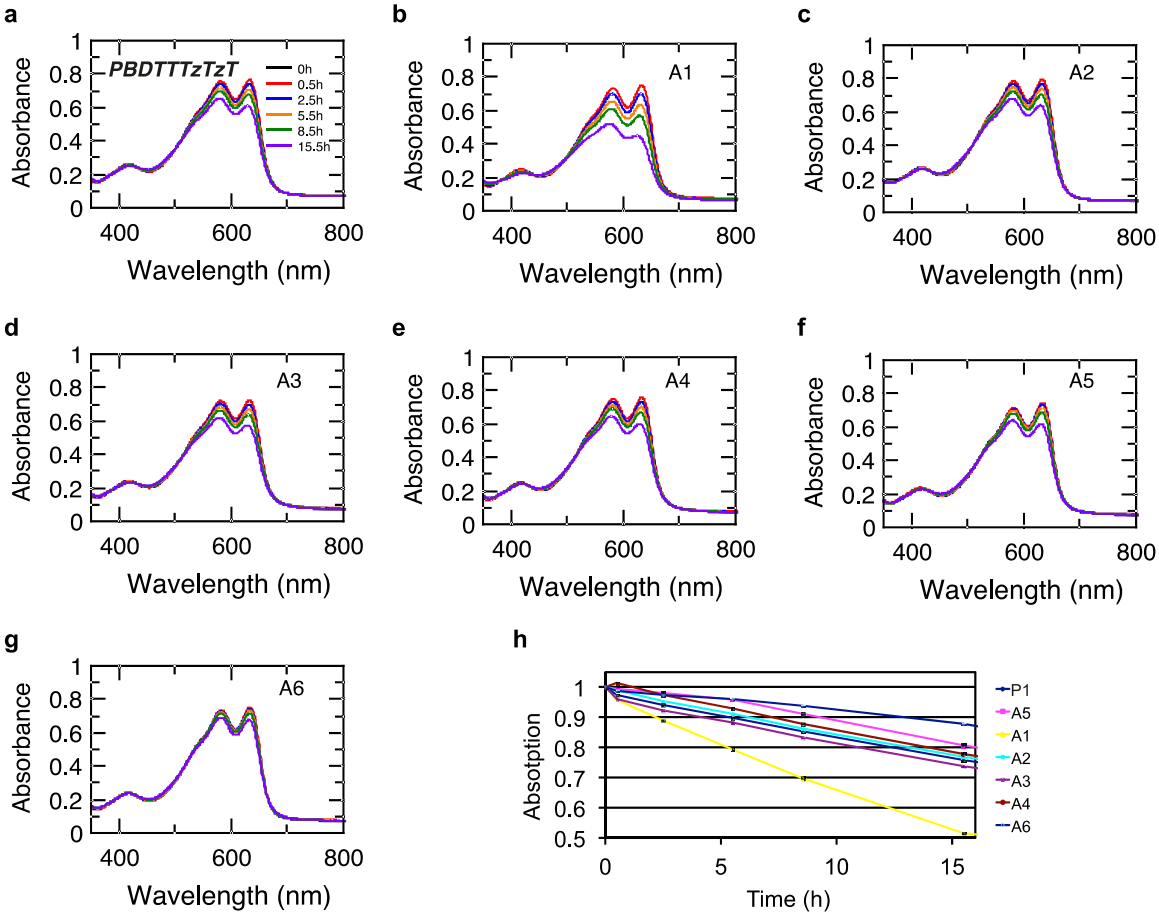

Figure S7. Reaction spectra of PBDTTTzTzT films. a, neat PBDTTTzTzT, **b – g**, PBDTTTzTzT films containing 10wt% of the antioxidants A1 – A6 exposed to a solar simulator in air. **h**, Photooxidation kinetics of PBDTTTzTzT films in the absence (R)/ presence of the additives A1 – A6.

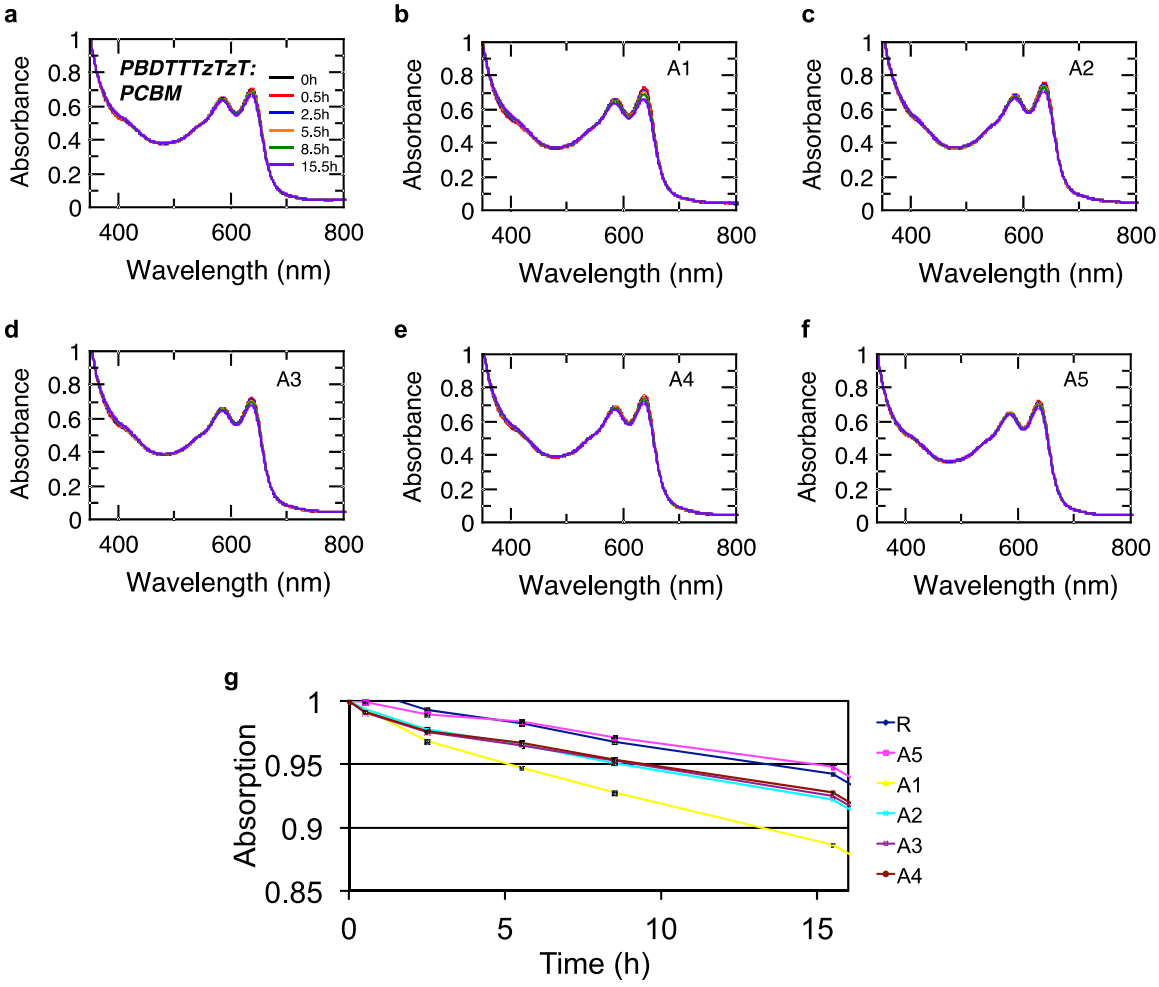

Figure S8. Reaction spectra of PBDTTTzTzT:PC60BM blend films. a, PBDTTTzTzT:PC60BM, **b – f**, PBDTTTzTzT:PC60BM films containing 10wt% of the antioxidants A1 – A5 exposed to a solar simulator in air. **g**, Photooxidation kinetics of PBDTTTzTzT:PC60BM films in the absence (R)/ presence of the additives A1 – A5.

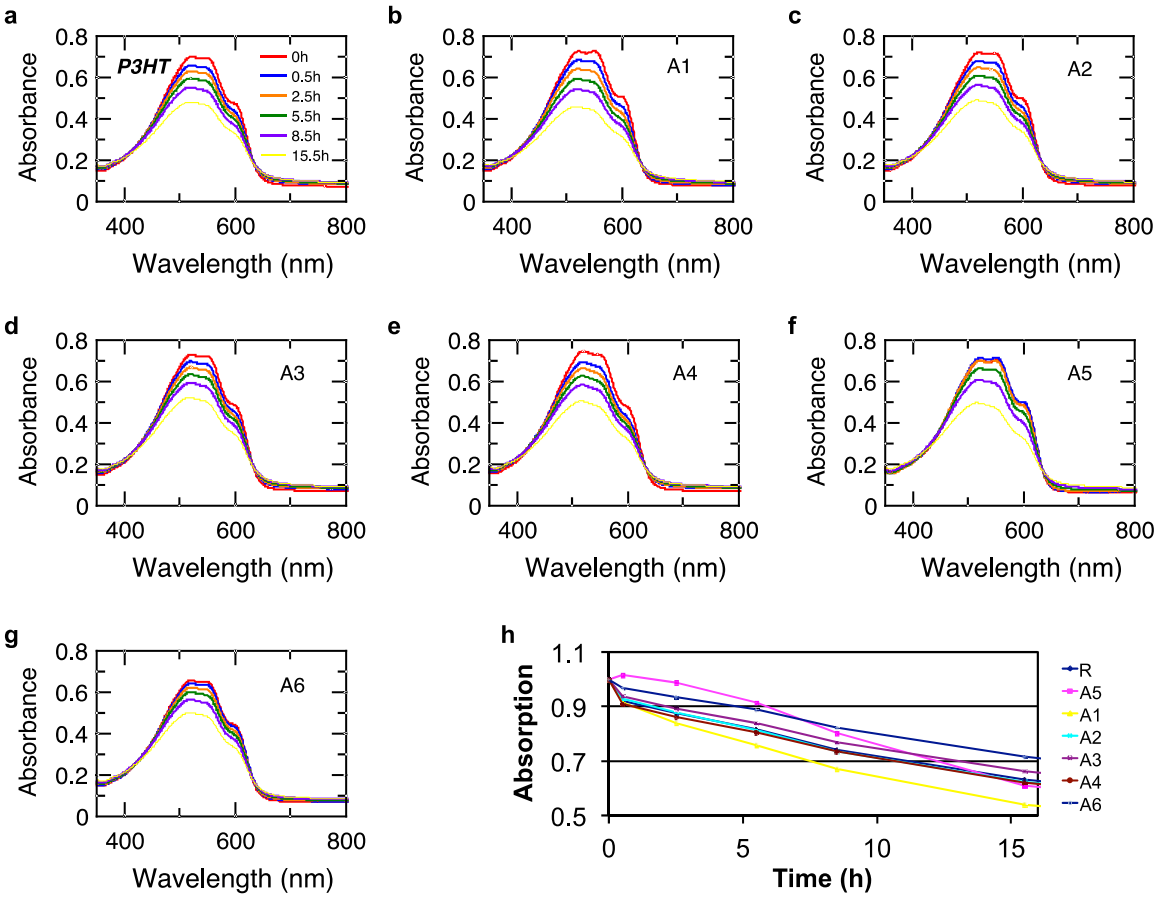

Figure S9. Reaction spectra of P3HT films. a, neat P3HT, **b – g**, P3HT films containing 10wt% of the antioxidants A1 – A6 exposed to a solar simulator in air. **h**, Photooxidation kinetics of P3HT films in the absence (R)/ presence of the additives A1 – A6.

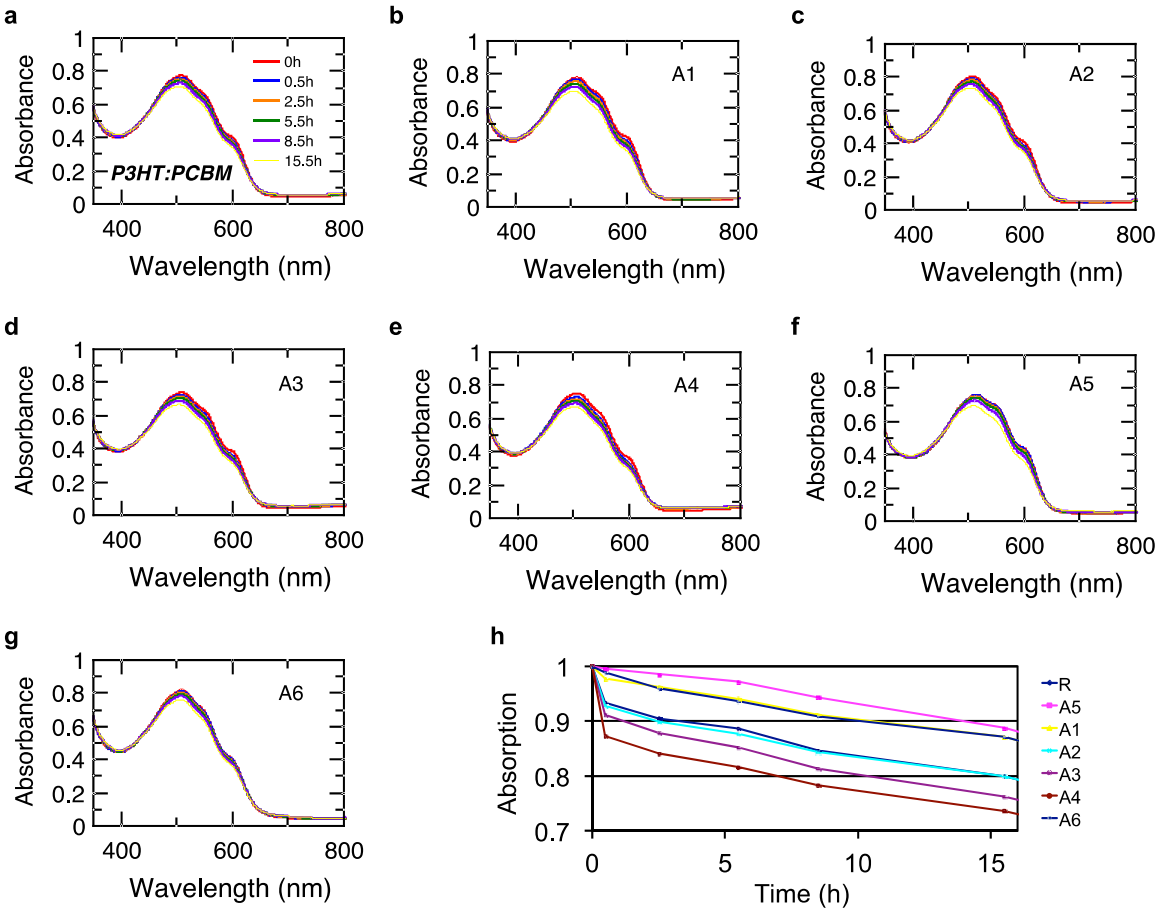

Figure S10. Reaction spectra of P3HT:PC60BM blend films. a, P3HT:PC60BM, **b – f**, P3HT:PC60BM films containing 10wt% of the antioxidants A1 – A5 exposed to a solar simulator in air. **g**, Photooxidation kinetics of P3HT:PC60BM films in the absence (R)/ presence of the additives A1 – A5.

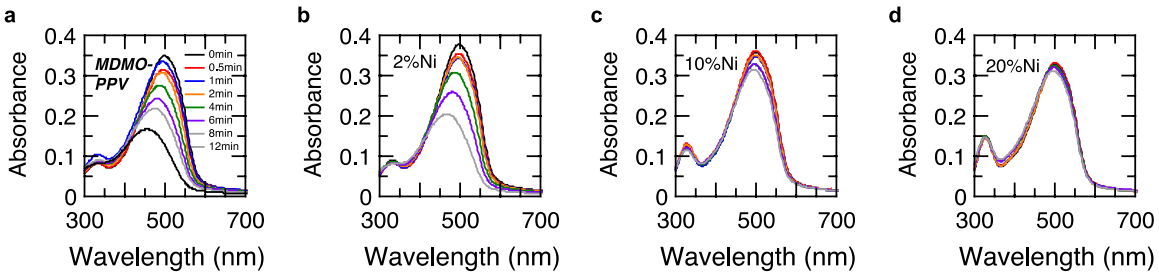

Figure S11. Reaction spectra of MDMO-PPV films. a, neat MDMO-PPV, **b – d,** MDMO-PPV films containing 2, 10, 20wt% of $Ni(dtc)_2$ (abbreviated to Ni) exposed to a solar simulator in air.

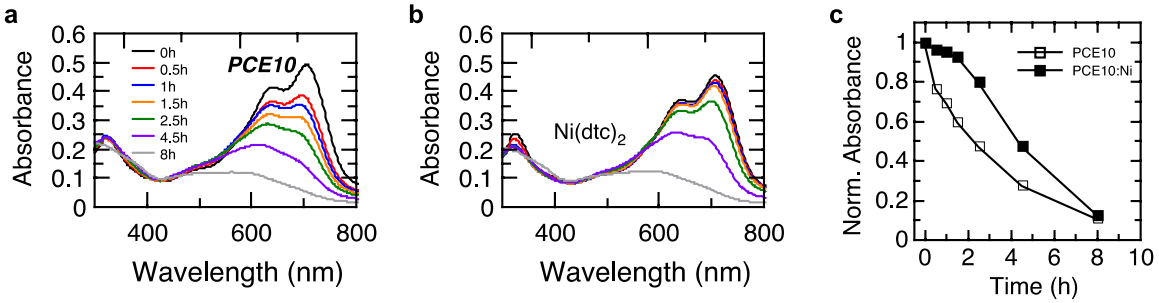

Figure S12. Reaction spectra of PTB7-Th (PCE10) films. a, neat PTB7-Th (PCE10) and **b,** PTB7-Th (PCE10) film containing 10wt% of $Ni(dtc)_2$ exposed to a solar simulator in air. **c**, Photooxidation kinetics of PTB7-Th films in the absence / presence of $Ni(dtc)_2$ (abbreviated to Ni).

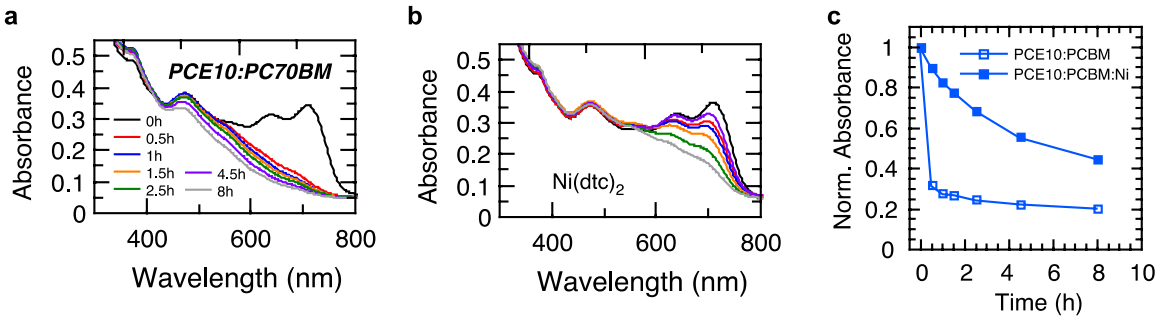

Figure S13. Reaction spectra of PTB7-Th (PCE10):PC70BM films. a, PTB7-Th:PC70BM and **b,** PTB7- Th:PC70BM film containing 4wt% of $Ni(dtc)_2$ (wrt blend) exposed to a solar simulator in air. **c**, Photooxidation kinetics of PTB7-Th:PC70BM films in the absence / presence of $Ni(dtc)_2$ (abbreviated to Ni).

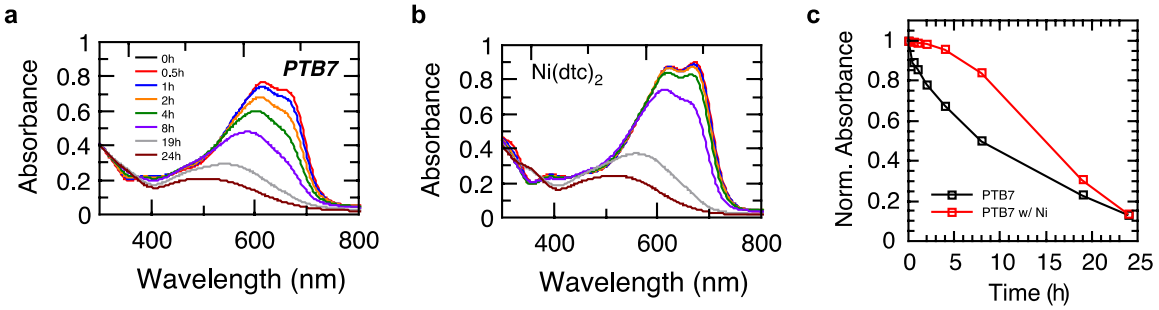

Figure S14. Reaction spectra of PTB7 films. a, neat PTB7 and **b,** PTB7 film containing 10wt% of $Ni(dtc)_2$ exposed to a solar simulator in air. **c**, Photooxidation kinetics of PTB7 films in the absence / presence of $Ni(dtc)_2$ (abbreviated to Ni).

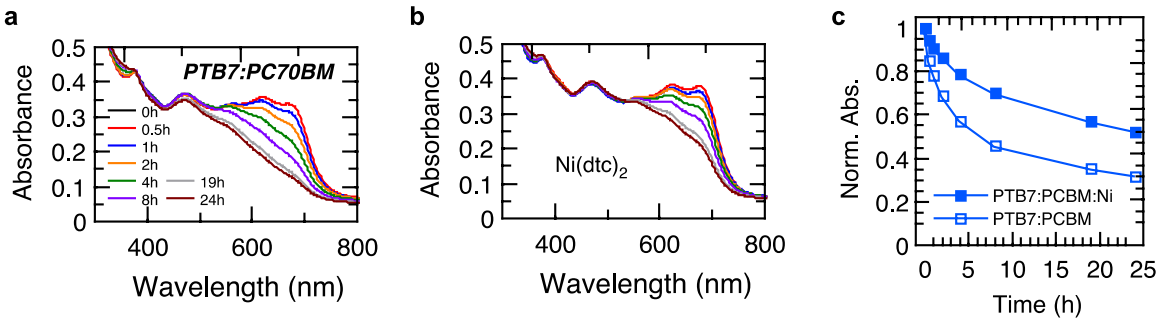

Figure S15. Reaction spectra of PTB7:PC70BM films. a, PTB7:PC70BM and **b,** PTB7- Th:PC70BM film containing 4wt% of $Ni(dtc)_2$ (wrt blend) exposed to a solar simulator in air. **c**, Photooxidation kinetics of PTB7-Th:PC70BM films in the absence / presence of $Ni(dtc)_2$ (abbreviated to Ni).

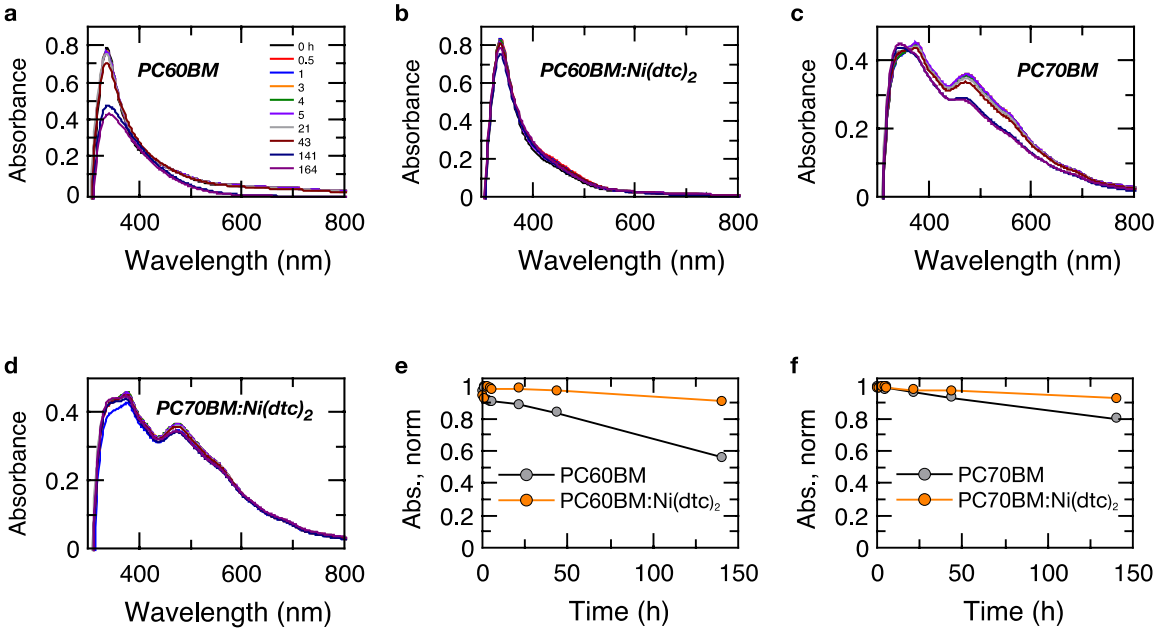

Figure S16. Reaction spectra of PCBM films. a, PC60BM and **b,** PC60BM:$Ni(dtc)_2$, **c**, PC70BM and **d**, PC60BM:$Ni(dtc)_2$ exposed to a solar simulator in air. **e,** and **f**, Photooxidation kinetics of PC60BM and PC70BM films in the absence / presence of $Ni(dtc)_2$ (10wt%) probed at 340 and 476 nm, respectively.

Table S1. Level of stabilization imposed by antioxidants. The polymers 1 – 7 were probed without and with 50% (w/w) PCBM (66% in the case of PTB7 and PTB7-Th) by the stabilizers 1 – 6 (+++/++/+ high/medium/low level of stabilization, O no effect, - destabilization)

		1	**2**	**3**	**4**	**5**	**6**
1	Neat PBDTTTzTzT	-	O	O	O	++	++
	+ PC60BM	-	O	O	O	+	+
2	Neat P3HT	-	O	O	O	+	+
	+ PC60BM	O	O	O	O	O	+
3	Neat PCPDTBT	O	O	O	O	++	O
	+ PC60BM	O	O	O	O	+++	O
4	Neat SiPCPDTBT	O	O	+	O	+	O
	+ PC60BM	O	O	O	O	O	O
5	Neat PTB7	O	tbd	tbd	tbd	++	tbd
	+ PC70BM	O	tbd	tbd	tbd	+++	tbd
6	Neat PTB7-Th	O	tbd	tbd	tbd	++	tbd
	+ PC70BM	O	tbd	tbd	tbd	+++	tbd
7	MDMO-PPV	tbd	tbd	tbd	tbd	+++	tbd

Derivation of figure of merit (FOM) for categorizing the effectiveness of stabilizers

We define the FOM of stabilizers as the moles of monomer units of a polymer saved from photo-oxidation by addition of a stabilizer per moles stabilizer lost.

The FOM may be calculated from the reaction spectra, inserting the absorption losses for both polymer and stabilizer, after a certain time Δt of irradiation:

$$FOM(\Delta t) = \frac{\varepsilon(Ni) \cdot [\Delta E(polymer\ w/o\ Ni) - \Delta E(polymer\ w\ Ni)]}{\varepsilon(monomer\ unit) \cdot \Delta E(Ni)} \quad \text{(S1)}$$

Where ΔE(polymer w/o Ni) and ΔE(polymer w Ni) mean the decreases of absorbance of the polymer without and with the stabilizer, respectively, and ΔE(Ni) denotes the decrease of absorbance of the Ni complex. ε(monomer unit) and ε(Ni) are the molar extinction coefficients of a monomer unit of the polymer and of the stabilizer, respectively. The molar extinction coefficient of the band at 330 nm of the Ni complex is approximately (from the absorption spectrum of the P3HT:Ni(dtc)$_2$ film):

$$\varepsilon(Nidtc2) = \varepsilon(polymer) \cdot \frac{E(Nidtc2)}{E(polymer)} \cdot x^{-1}(Nidtc2) \approx 10^4 cm^2 \cdot mmol^{-1} \cdot \frac{0.09}{0.9} \cdot 34.5 = 3$$

Equation (S1) can be rearranged, yielding

$$FOM(\Delta t) = \frac{x(polymer) \cdot \left[\Delta E\left(polymer\frac{w}{o}Ni\right) - \Delta E(polymer\ w\ Ni)\right] / E(polymer, t=0)}{x(Nidtc2) \cdot \Delta E(Ni)/E(Ni, t=0)} =$$

$$\frac{x(polymer)\cdot \Delta\Delta E(polymer)/E(polymer,t=0)}{x(Nidtc2)\cdot \Delta E(Ni)/E(Ni,t=0)} =$$

$$\frac{[1-x(Nidtc2)]\cdot \Delta\Delta E(polymer)/E(polymer,t=0)}{x(Nidtc2)\cdot \Delta E(Ni)/E(Ni,t=0)} \qquad \text{(S2)}$$

Where x(polymer) and x(Nidtc2) are the mole fractions of monomer units of the polymer and of the Ni complex, respectively. The mole fraction of $Ni(dtc)_2$ in a given film is

$$x(Nidtc_2) = \frac{n(Nidtc2)}{n(Nidtc2)+n(polymer)} = \frac{m(Nidtc2)/M(Nidtc2)}{m(Nidtc2)/M(Nidtc2)+m(polymer)/M(polymer)}$$

Where m(Nidtc2) and m(polymer) are the masses of the Ni complex and of the polymer in the film, respectively. M(Nidtc2) and M(polymer) are the molar masses of the Ni complex and of a monomer unit of the polymer, respectively. For a film containing 10% w/w of $Ni(dtc)_2$, this becomes

$$x(Nidtc_2) = \frac{1}{1+\frac{m(polymer)/M(polymer)}{m(Nidtc2)/M(Nidtc2)}} = \frac{1}{1+9\cdot\frac{M(Nidtc2)}{M(polymer)}} =$$

$$\frac{1}{1+9\cdot\frac{622{,}7\ g\cdot mol^{-1}}{M(polymer)}}$$

The mole fractions for the four polymer:$Ni(dtc)_2$ blends are given in Tab.S2.

Inserting the values calculated for $x(Ni(dtc)_2)$ into eq. S2, along with the values of $\Delta\Delta E(polymer)$, $\Delta E(Ni)$, $E(polymer,t=0)$, and $E(Ni,t=0)$ extracted from the reaction spectra, the values of the respective FOM listed in Table S2 are obtained.

The following cases of FOM can be distinguished:

FOM >> 1: many monomer units saved before stabilizer molecule is lost

FOM = 1: for every monomer unit saved one stabilizer molecule is lost

0 < FOM < 1: stabilizer still stabilizes, but is more sensitive to oxidation than polymer

FOM < 0: “stabilizer” destabilizes polymer

Table S2. Parameters leading to the figure of merit of $Ni(dtc)_2$ for stabilizing conjugated polymer.

polymer	**P3HT**	**PTB7-Th**	**PTB7**	**PCPDTBT**
M / g mol^{-1}	166	860	728	534
x($Nidtc_2$)	0.029	0.133	0.115	0.087
$\Delta t/min$	240	150	240	240
$\Delta E(Ni)*$	0.08	0.04	0.07	0.015
$E(Ni, t=0)*$	0.09	0.04	0.07	0.06
$\Delta\Delta E(polymer)$	0.01	0.32	0.28	0.033
$E(polymer, t=0)$	1	1	1	1
FOM per monomer unit	0.5	2.1	2.2	1.5
FOM per double bond	1	12.6	13.2	9.0

*values relative to the normalized maximum absorbance of the polymer before degradation, $E(polymer, t=0)$.

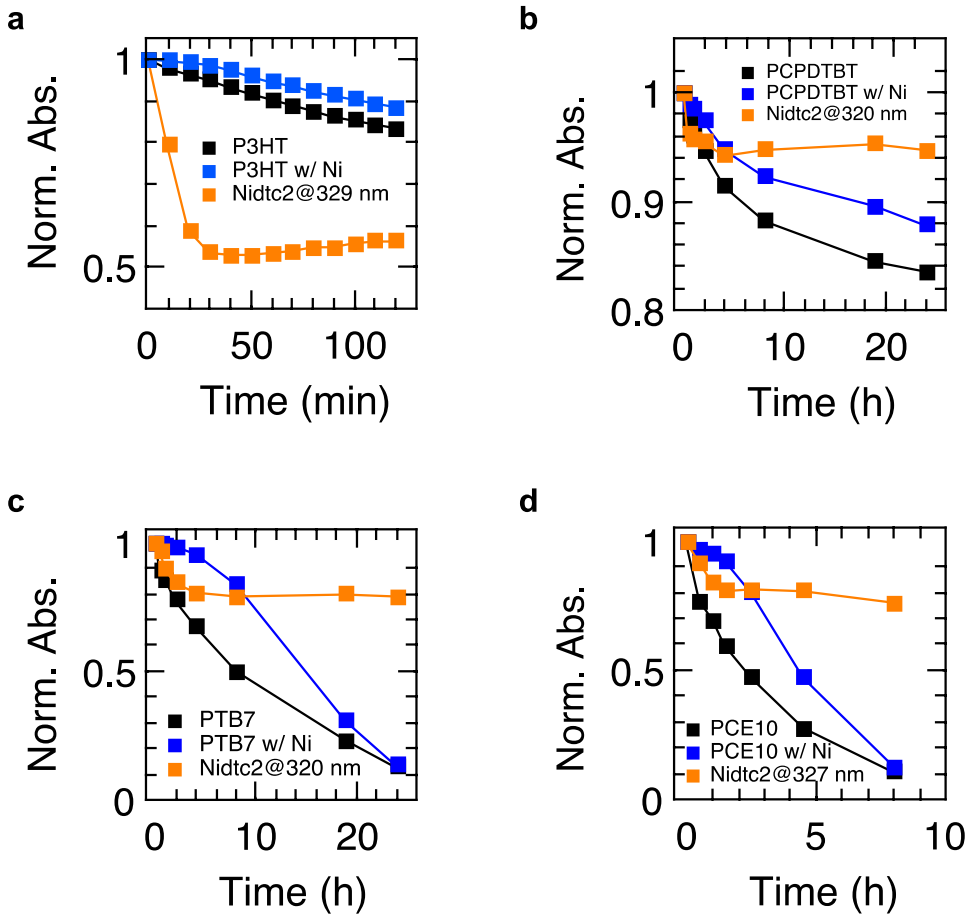

Figure S17. Photo-oxidation kinetics of conjugated polymers used for estimating the figure of merit (FOM) of the stabilizer $Ni(dtc)_2$. a, P3HT, **b**, PCPDTBT, **c**, PTB7 and d, PTB7-Th (PCE10).

Electrons spin resonance spectroscopy of conjugated polymers, blends and fullerenes

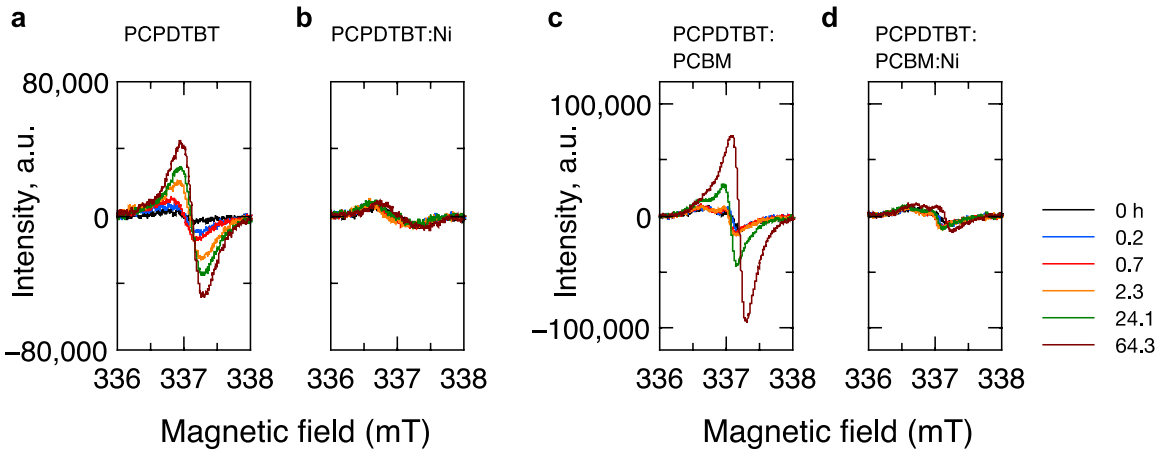

Figure S18. Temporal evolution of X-Band ESR spectra of PCPDTBT. a, PCPDTBT, **b**, PCPDTBT:Ni(dtc)$_2$ (1:0.15), **c**, PCPDTBT:PC60BM (1:1) and **d**, PCPDTBT: PC60BM: Ni(dtc)$_2$ (1:1:0.15) exposed to white light irradiation (~80 mW/cm^2) in air.

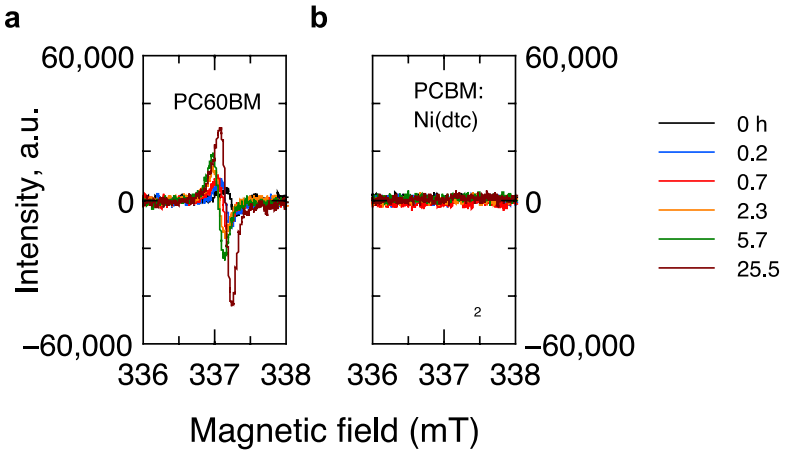

Figure S19. Temporal evolution of X-Band ESR spectra of PC60BM. a, PC60BM and **b**, PC60BM:Ni(dtc)$_2$ (1:0.15) exposed to white light irradiation (~80 mW/cm^2) in air.

Singlet oxygen ($^1O_2$) sensitization experiments using singlet oxygen sensor green (SOSG)

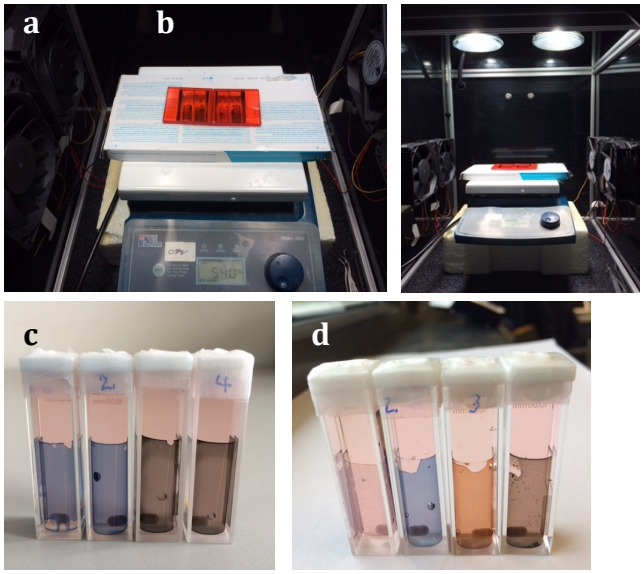

Figure S20. Experimental setup for probing singlet oxygen formation using the sensor singlet oxygen sensor green (SOSG). a, Films of polymer and polymer:fullerene blends on PET foil were folded into quartz cuvettes and immersed in a solution of SOSG. The cuvettes were exposed to solar simulator light using a 570 nm cut off filter. The solutions were continuously stirred. **b**, Overview of the light soaking setup. **c** and **d**, Photographs of films of PTB7-Th and PTB7-Th:PC70BM on PET foil immersed in SOSG solution before and after 120 min of white light irradiation, respectively. From left to right: PTB7-Th, PTB7-Th:$Ni(dtc)_2$, PTB7-Th:PC70BM, PTB7-Th:PC70BM:$Ni(dtc)_2$. The amount of $Ni(dtc)_2$ was 10wt% with respect to the polymer (4wt% in the blends).

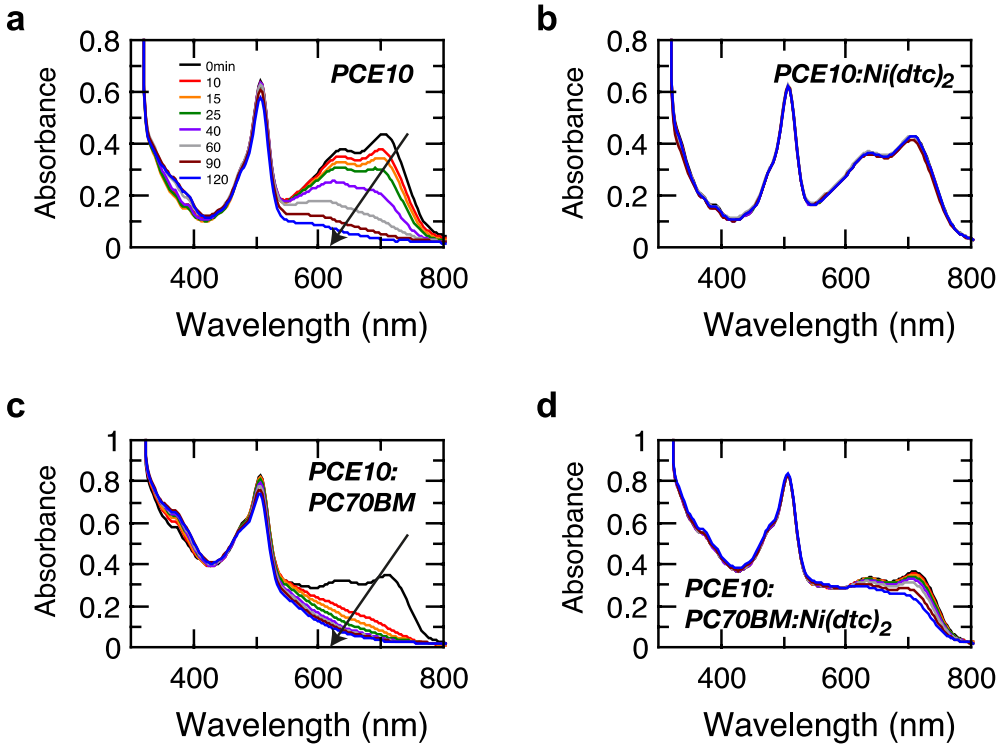

Figure S21. Reaction spectra of photo-oxidized films of PTB7-Th (PCE10) immersed in SOSG solution. a, neat PTB7-Th, **b**, PTB7-Th:Ni(dtc)$_2$, **c**, PTB7-Th:PC70BM and **d**, PTB7-Th:PC70BM:Ni(dtc)$_2$ exposed to a solar simulator in air. The films were spin coated on PET foil and immersed in a solution of singlet oxygen sensor green (absorption maximum around 500 nm) inside a quartz cuvette. The UV-VIS spectra were taken through the cuvette. The arrows indicate the increase in photo-bleaching with increasing photo-oxidation time.

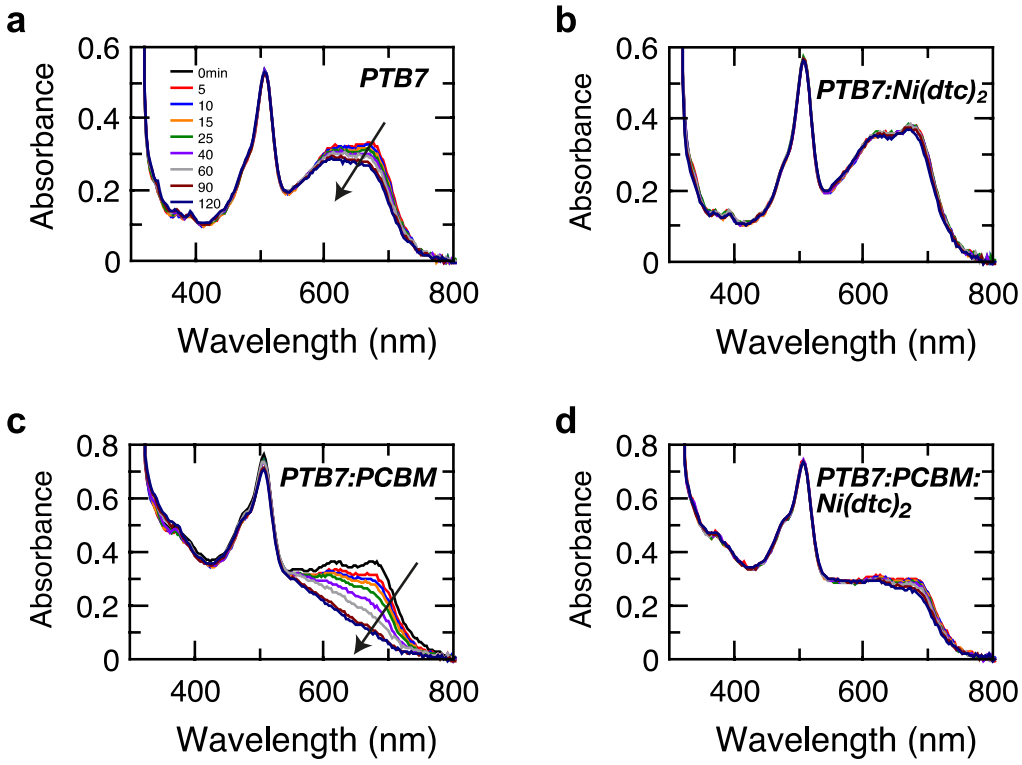

Figure S22. Reaction spectra of photo-oxidized films of PTB7 immersed in SOSG solution. **a,** neat PTB7, **b**, PTB7:Ni(dtc)$_2$, **c**, PTB7:PC70BM and **d**, PTB7:PC70BM:Ni(dtc)$_2$ exposed to a solar simulator in air. The films were spin coated on PET foil and immersed in a solution of singlet oxygen sensor green (absorption maximum around 500 nm) inside a quartz cuvette. The UV-VIS spectra were taken through the cuvette. The arrows indicate the increase in photo-bleaching with increasing photo-oxidation time.

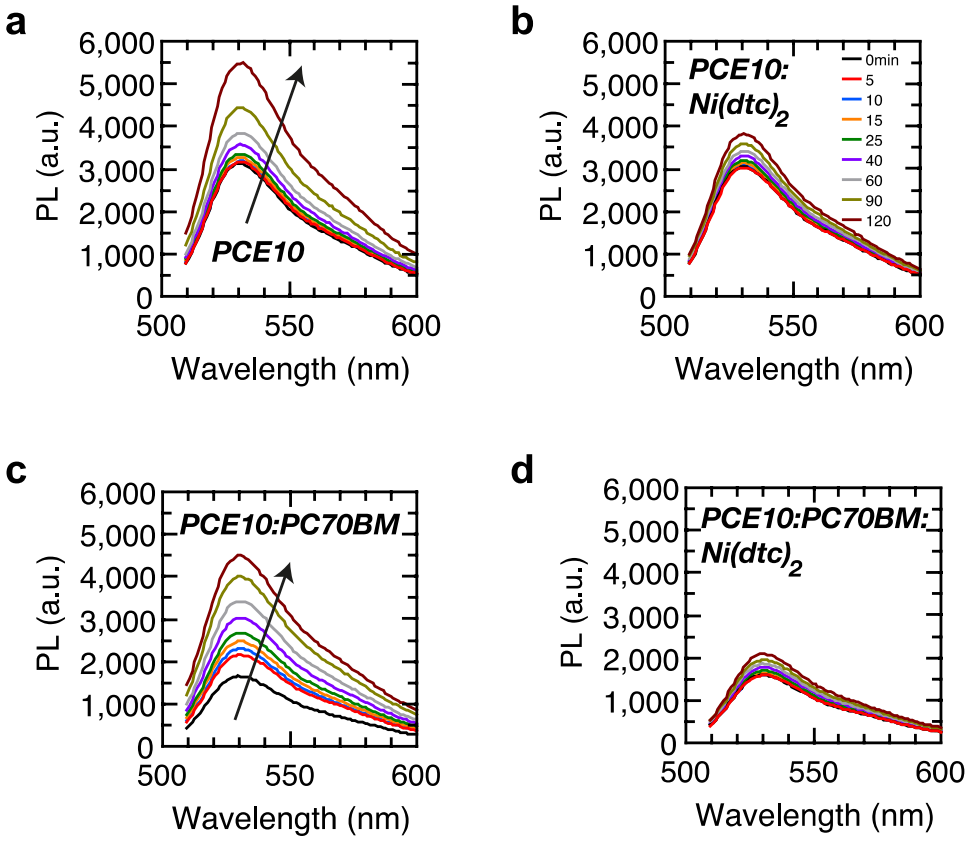

Figure S23. Photoluminescence spectra of SOSG solution in contact with photo-oxidized films of PTB7-Th. a, neat PTB7-Th (PCE10), **b**, PTB7-Th:Ni(dtc)$_2$, **c**, PTB7-Th:PC70BM and **d**, PTB7-Th:PC70BM:Ni(dtc)$_2$ exposed to a solar simulator in air (485 nm excitation and 490 nm cutoff in front of detector). The same films / cuvettes where used as in Figure S20. The arrows indicate the increase in photoluminescence with increasing photo-oxidation time.

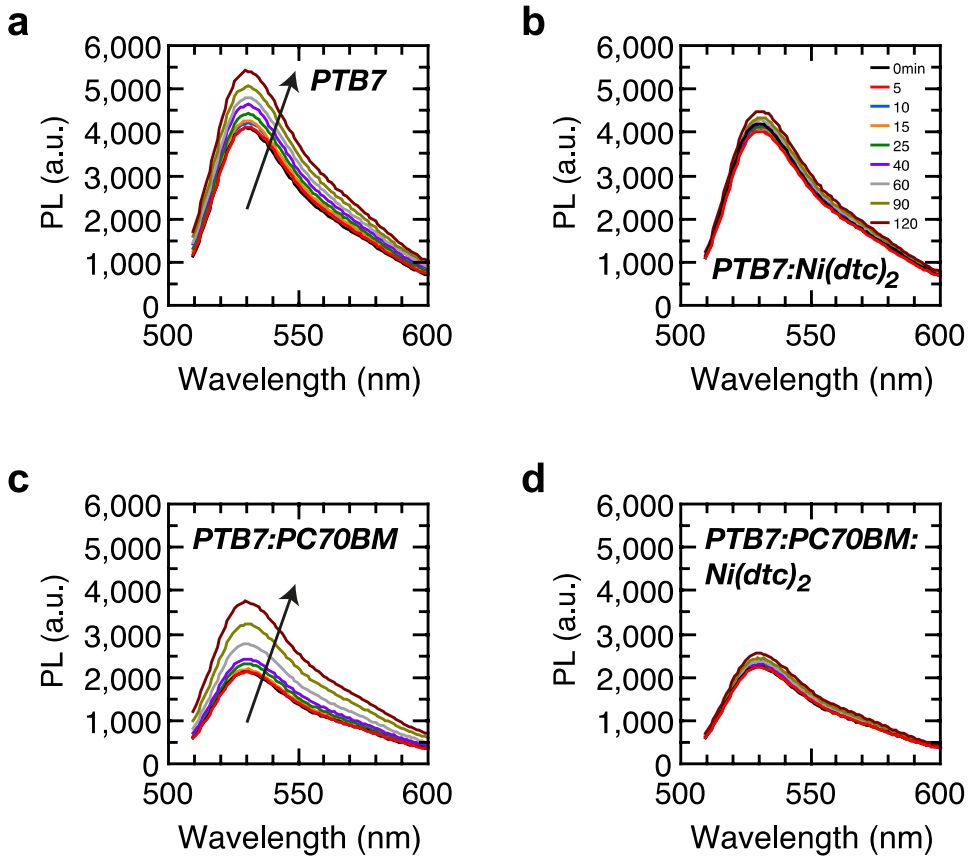

Figure S24. Photoluminescence spectra of SOSG solution in contact with photo-oxidized films of PTB7. a, neat PTB7, **b**, PTB7:Ni(dtc)$_2$, **c**, PTB7:PC70BM and **d**, PTB7:PC70BM:Ni(dtc)$_2$ exposed to a solar simulator in air (485 nm excitation and 490 nm cutoff in front of detector). The same films / cuvettes where used as in Figure S21. The arrows indicate the increase in photoluminescence with increasing photo-oxidation time.

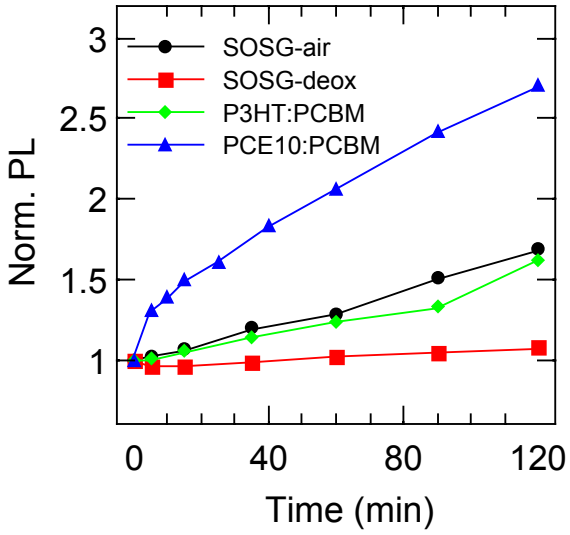

Figure S25. Kinetics of the fluorescence signal amplitude of SOSG solutions as a function of irradiation time (under solar simulator). The traces correspond to a SOSG solution prepared in air (black circles), a deoxygenated SOSG control solution (red squares) and a SOSG solution in contact with films of P3HT:PCBM (green diamonds) and PTB7-Th:PC70B (blue triangles). The increasing PL signal reflects the accumulated formation of $^1O_2$.

Photoluminescence detection of singlet oxygen in polymer blend films

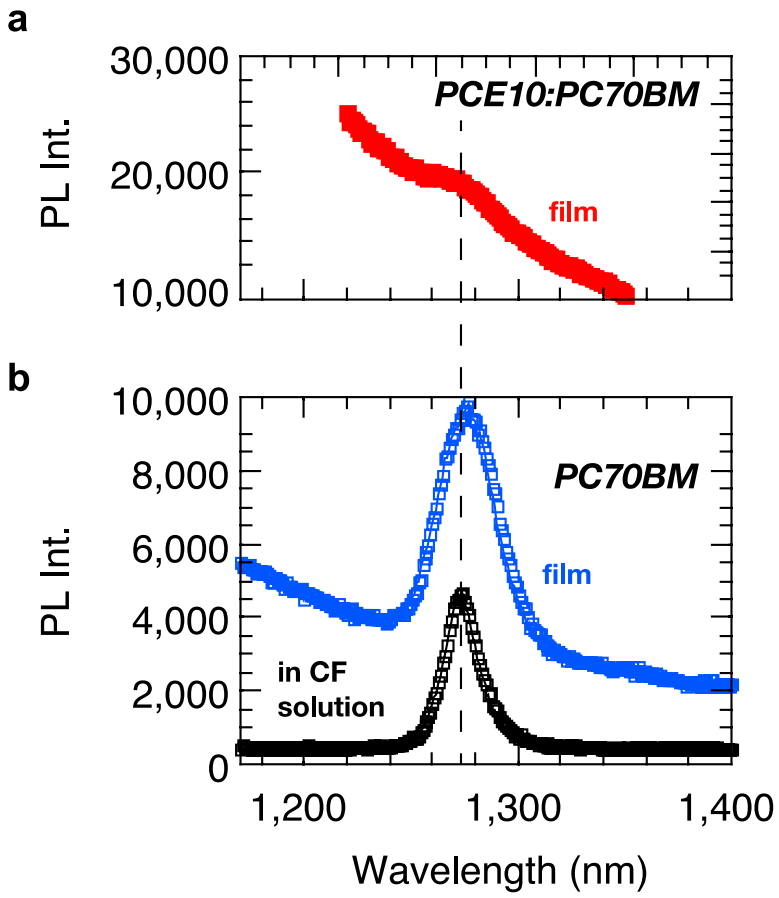

Figure S26. Spectroscopic signatures of singlet oxygen in film and solution. a, Photoluminescence of a spin coated film of PCE10:PCBM and **b**, photoluminescence of a spin coated film of PC70BM and of PC70BM in solution (chloroform) upon 405 nm laser light excitation.

Low-temperature photo-induced absorption and photoluminescence spectroscopy on films of PCE10:Ni(dtc)$_2$

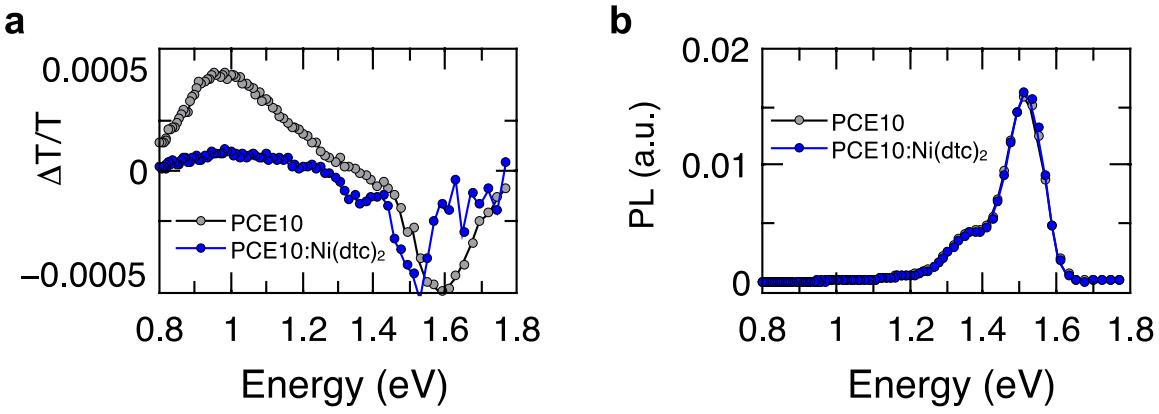

Figure S27. Photo-induced absorption and photoluminescence spectra of PTB7-Th at 10K. a, Photo-induced absorption of neat PTB7-Th (PCE10) and PTB7-Th:Ni(dtc)$_2$ (10wt%). Positive $-\Delta T/T$ values mean an increase in absorption, while negative $-\Delta T/T$ values represent an increase in transmission (bleach). **b**, photoluminescence spectra of neat PTB7-Th (PCE10) and PTB7-Th:Ni(dtc)$_2$. In both cases we used 530 nm laser light excitation (160 Hz). The signal at 1 eV has been previously assigned to triplet state transitions in the case of PTB7.[1]

Triplet quenching in PTB7 thin films with and without $Ni(dtc)_2$, in oxygen and vacuum

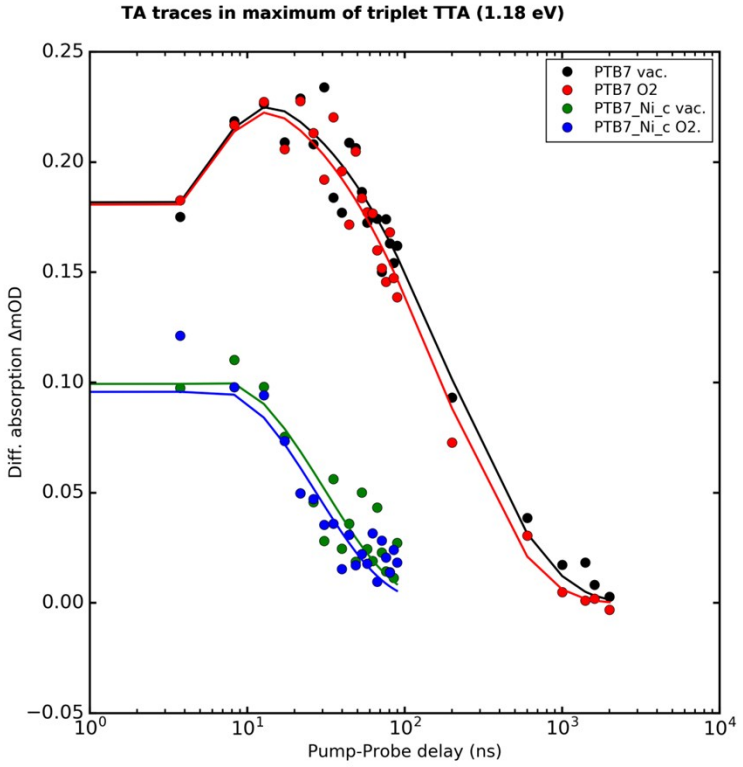

Figure S28. Transient absorption spectra of films of PTB7 and PTB7:$Ni(dtc)_2$. Films of PTB7 with and without $Ni(dtc)_2$ (10wt%) were probed in ambient air and under vacuum at a probe energy of 1.18 eV, close the maximum of triplet-triplet absorption. All samples were pumped at 532 nm with a 300 ps laser with fluence of 41 μJ cm^{-2}. Solid lines are results of a global fit using the model given in the text.

Figure S28 shows transient absorption (TA) traces of PTB7, close to the maximum of the triplet absorption band. In the absence of $Ni(dtc)_2$, an initial rise of the TA signal reflects the instrumental time constant of our setup at about 13 ns (one order of magnitude better

than in previous reports[2]). To conserve the full time resolution, no binning was applied along the time axis, resulting in substantial noise in the nanosecond time range. However, the microsecond range, we reach a noise level below 10^{-5} ΔOD, which allows us to clearly observe accelerated triplet quenching in the presence of oxygen compared to vacuum, compare red and black symbols, respectively.

If the Nickel complex is present, triplet quenching is accelerated by about one order of magnitude, see green and blue symbols.

To obtain rate constants, we applied a kinetic global fitting. We found that a simple monoexponential decay scheme does not reproduce the triplet decay in the absence of $Ni(dtc)_2$, in agreement with the qualitative findings from Soon et al.[2] We therefore include a bimolecular triplet annihilation term,

$$\frac{dT}{dt} = g - k_a T^2 - (k_{m,intr} + k_{m,ox} + k_{m,Nic})T \quad (1)$$

Here, k_a, $k_{m,intr}$ and $k_{m,\ ox}$ are the rate constants for bimolecular annihilation and monomolecular deactivation, respectively, of triplet state at concentration T by intrinsic mechanisms, molecular oxygen and the Nickel complex, respectively. The generation term g is assumed as a Gaussian of 13 ns duration. We globally fitted PTB7 under vacuum and oxygen with all parameters free (except $k_{m,\ Nic}$ which was set to zero). Then we fixed k_a and $k_{m,intr}$ and globally fitted PTB7 with the Nickel complex in vacuum and oxygen. Table 1 shows the results.

Inserting Lambert-Beer's law into eq.1 yields

$$\frac{dA}{dt} = g \cdot \sigma d - \frac{k_a}{\sigma d}A^2 - (k_{m,intr} + k_{m,ox} + k_{m,Nic})A, \quad (2)$$

where A is the differential absorption at probe energy $\omega_{pr} = 1.18$ eV, σ the absorption cross-section at that probe energy, and d the sheet thickness. The term $k_a^{'} = k_a/\sigma d$ is called the spectroscopic rate constant.

Table S3. Results from global fitting of TA spectra (vacuum and oxygen measurements fitted together). An asterisk (*) indicates that the respective value was fixed in the fit. Values in brackets are standard deviations of the last digit. The bimolecular annihilation constant k_a is given as spectroscopic rate constant.

Sample	k_a * / ns^{-1}	$k_{m,intr}$ / ns^{-1}	$k_{m,ox}$ / ns^{-1}	$k_{m,Nic}$ / ns^{-1}
PTB7	6(1)	0.0021(4)	0.0008(2)	0*
PTB7 / $Ni(dtc)_2$	6(1)*	0.0021*	0.003(1)	0.031(1)

From Table 1, we see that $Ni(dtc)_2$ outperforms oxygen-induced triplet quenching by more than an order of magnitude. However there is an inconsistency of the oxygen-induced quenching rate, which comes out a factor of three higher when the Nickel complex is present. This result needs to be confirmed by further measurements. With the data at hand, we consider the value obtained without $Ni(dtc)_2$ more reliable because in this case, the data points with and without oxygen are clearly separated, at least in the microsecond range.

Pump intensity dependence

Figure S29 shows Nanosecond TA traces for PTB7 in vacuum at two different pump intensities, measured directly after each other. These data clearly show that the fast initial decay is intensity dependent, therefore the assignment of a bimolecular rate constant is justified.

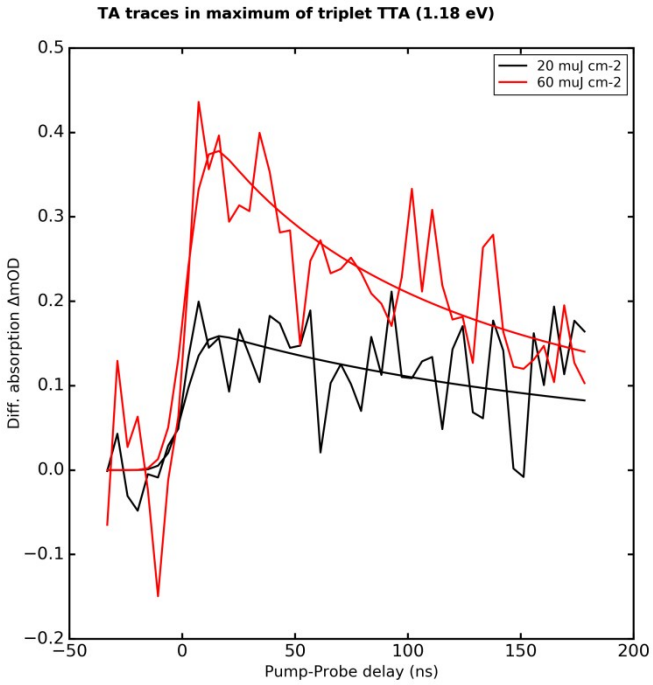

Figure S29. Pump intensity dependent triplet decay in PTB7 under vacuum. The spectra were taken upon pumping with a 532 nm 300 ps laser at the indicated pump intensities.

A global fit yields k_a^*=7.9(5) ns^{-1}, in reasonable agreement with the data in Table 1. Therefore we consider the observation of triplet annihilation as confirmed.

In order to get the bimolecular rate constant from the spectroscopic one, let us estimate the triplet concentration. A photon at 532 nm has the energy $3.7 \cdot 10^{-19}$ J. At 60 µJ cm^{-2} we

obtain $1.6 \cdot 10^{14}$ photons per cm^2. If half of these are absorbed and the triplet yield is 30%, then we have a total area density of $2.4 \cdot 10^{13}$ cm^{-2} triplets. These give 0.001 of differential absorption (base e), so $\sigma = 4.1 \cdot 10^{-17}$ cm^2, a quite reasonable value for an allowed transition of 0.1 eV bandwidth. Assuming a thickness of 100 nm yields finally $k_a = 2.5 \cdot 10^{-12}$ cm^3/s.

At the starting concentration, the exclusion volume is $1/(2.4 \cdot 10^{18}$ $cm^{-3})$, i.e., a cube of 7 nm edge length. The triplet samples this volume within 150 ns. A starting concentration of $2.4 \cdot 10^{18}$ cm^{-3} is equivalent to $4 \cdot 10^{-3}$ M. Since in the case of annihilation, triplet mobility counts double, $4 \cdot 10^{-3}$ M of annihilating species are equivalent to $8 \cdot 10^{-3}$M of an A+B reaction where B is immobile. Considering the concentrations of $Ni(dtc)_2$ and O_2 to be approximately 0.25 M and 0.01 M, respectively, we can therefore expect that at these triplet concentrations, triplet annihilation is in competition with oxygen-induced triplet quenching but will be outperformed by quenching at the Ni complex, which is much higher concentrated. Note that the term $k_{m,Nic}A$ is implicitly referring to a bimolecular reaction (with reaction constant $k_{m,b}$) between the Nickel complex at concentration [Ni-C] and the excited state, $\frac{dA}{dt} = k_{m,b} \cdot [Ni - C]A$, such that the bimolecular reaction constant $k_{m,b} = \frac{k_{m,Ni}}{[Ni - C]} = \frac{0.031 ns^{-1}}{0.25M} = 0.12 M^{-1} ns^{-1}$.

Photovoltaic device performance of polymer-fullerene solar cells with $Ni(dtc)_2$ embedded in the active layer

PTB7:PC70BM based solar cells

Table S4. Time zero photovoltaic device parameter for PTB7:PC70BM based solar cells as a function of $Ni(dtc)_2$ content.

Experiment	Jsc/mAcm^{-2} (SD)	Voc/V (SD)	FF (SD)	PCE (SD)	Max. PCE
0wt%	15.3 (0.2)	0.738 (0.003)	0.71 (0.004)	8.0 (0.1)	8.0 (0.1)
2wt%	11.9 (1.0)	0.729 (0.002)	0.68 (0.02)	5.9 (0.4)	5.9 (0.4)
4wt%	10.7 (1.0)	0.728 (0.003)	0.63 (0.04)	4.9 (0.5)	4.9 (0.5)

SD: standard deviation calculated from an average of 10 devices

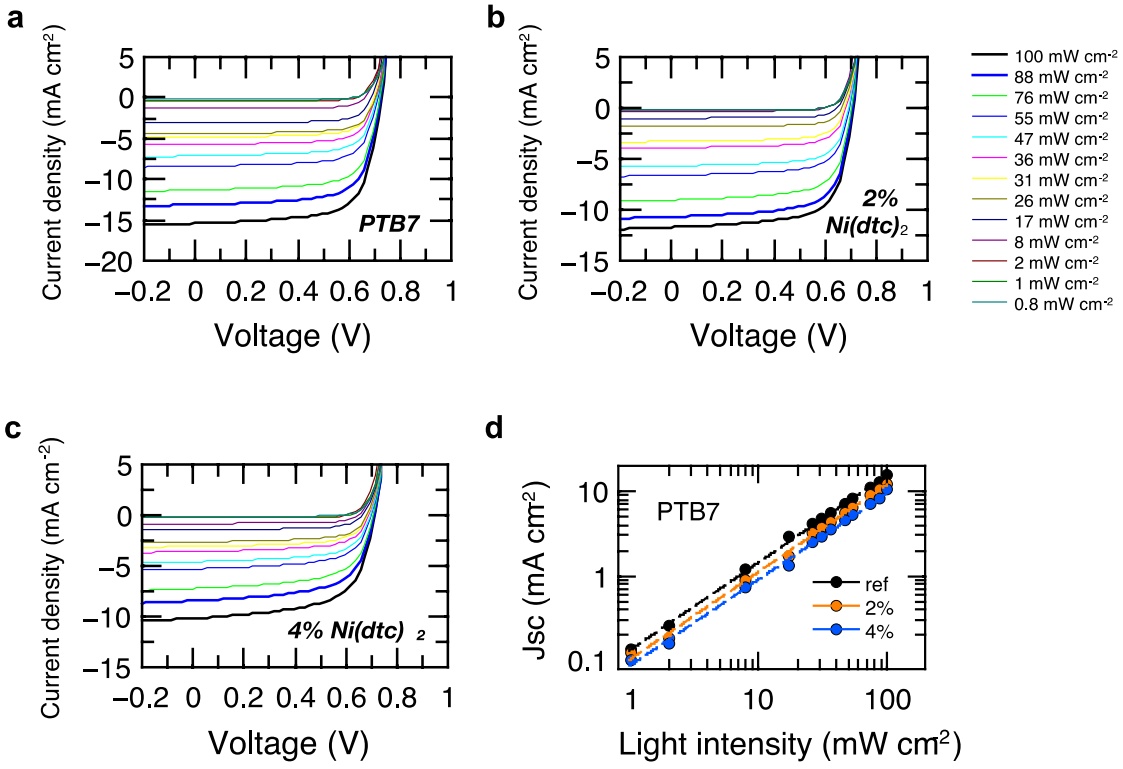

Figure S30. Light-intensity dependent current-voltage characteristics of PTB7:PC70BM based solar cells. a, PTB7:PC70BM-based solar cell, **b**, PTB7:PC70BM:$Ni(dtc)_2$ (2wt%) based solar cell, **c**, PTB7:PC70BM:$Ni(dtc)_2$ (4wt%) based solar cell. **d**, Double logarithmic representation of the short circuit current as a function of the light intensity for solar cells processed with and without $Ni(dtc)_2$. The slopes are 1.0 in all cases, indicating that $Ni(dtc)_2$ does not affect bimolecular recombination.

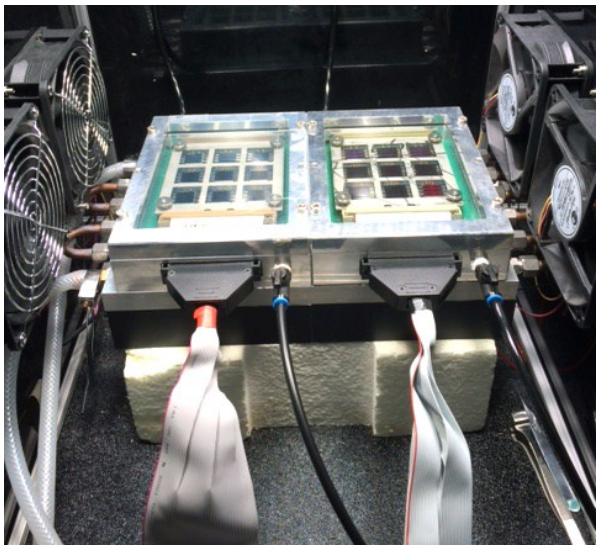

Figure S31. Photograph of the experimental chambers used for probing photo-oxidation of solar cell devices. The devices were irradiated under a static pressure of dry, synthetic air using metal halide lamps (4x150 W) of the type 150R Solarlux Class B from Eye Lighting. The devices were maintained at a constant temperature of ~30 ^{o}C using active cooling from the bottom.

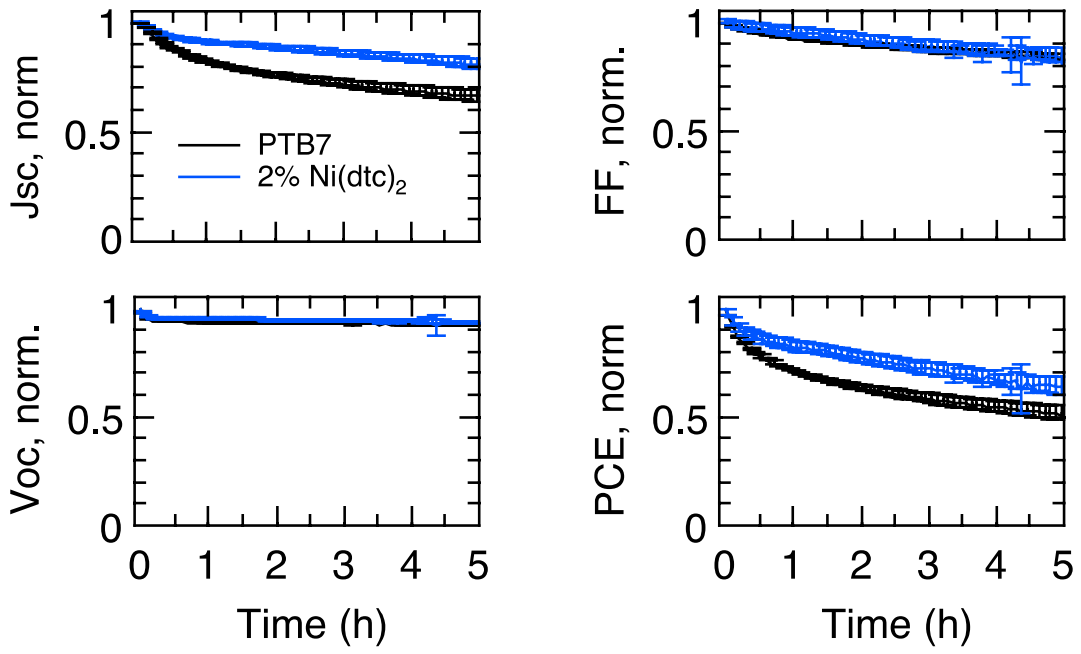

Figure S32. Temporal evolution of the photovoltaic parameters of PTB7:PC70BM solar cells with and without $Ni(dtc)_2$ under continuous light soaking. The traces represent averages from 10 devices.

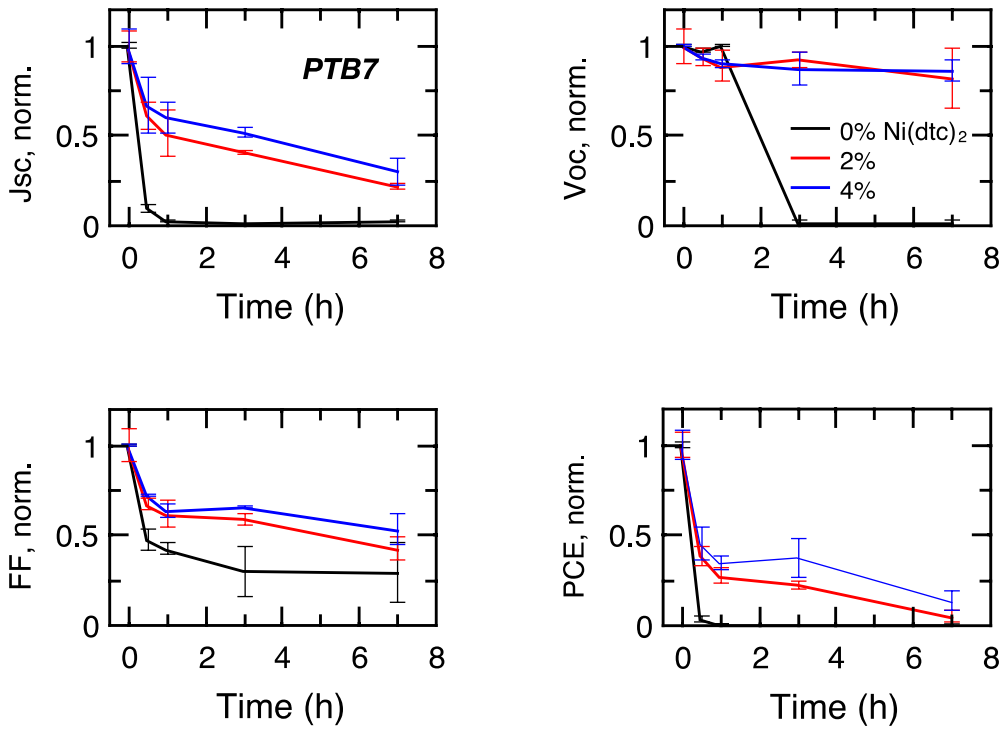

Figure S33. Photovoltaic parameters of PTB7:PC70BM half devices containing varying amounts of $Ni(dtc)_2$ as a function of time of exposure to solar simulator light. Half devices were fabricated up to the active layer and completed with a MoOx/Ag top electrode after light exposure. A UV blocking filter (Lithoprotect yellow foil Y520E212) was employed to filter UV radiation from the solar simulator.

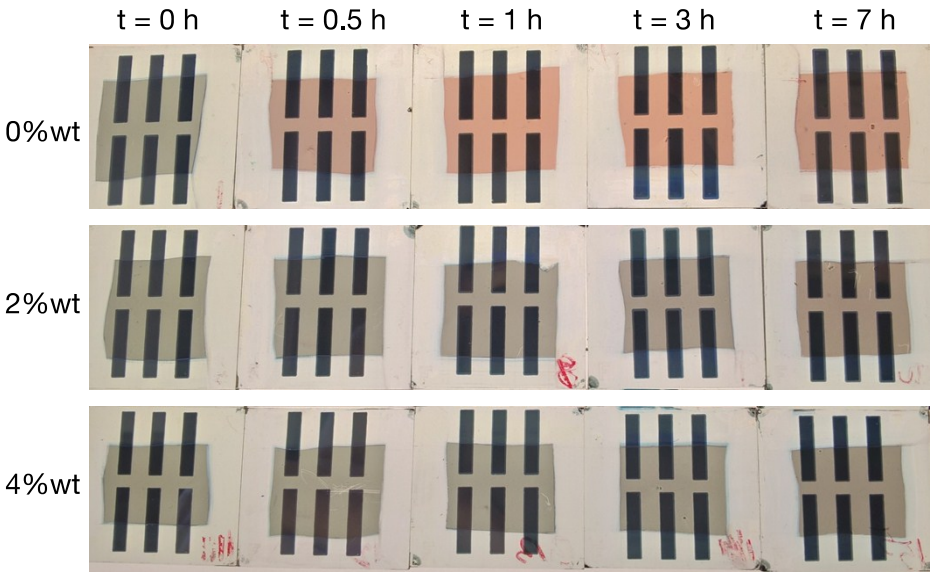

Figure S34. Photographs of photo-oxidized PTB7-based devices upon different times of exposure. The devices are the same as the ones characterized in Figure S31.

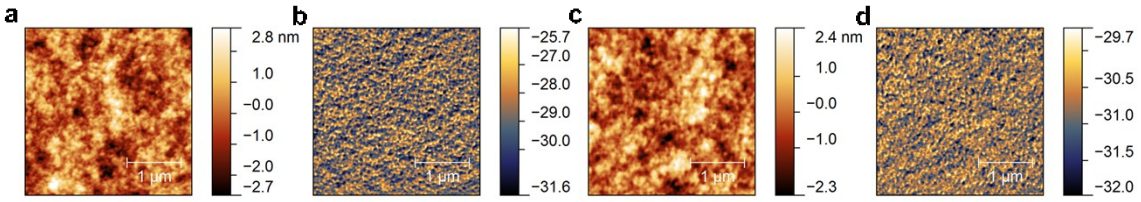

Figure S35. Intermittent contact atomic force micrographs of PTB7:PCB70BM active layers with and without 4wt% of $Ni(dtc)_2$. a, topography of PTB7:PCB70BM, **b**, AFM phase signal of PTB7:PCB70BM, **c**, topography of PTB7:PCB70BM:$Ni(dtc)_2$, **d**, AFM phase signal of PTB7:PCB70BM:$Ni(dtc)_2$.

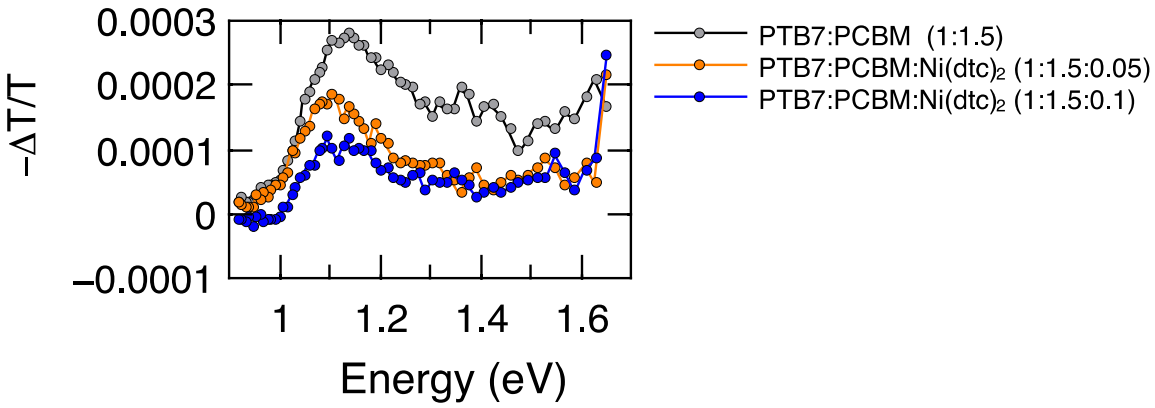

Figure S36. Room temperature photo-induced absorption spectra of PTB7:PC70BM films blended with different amounts of $Ni(dtc)_2$. Positive −ΔT/T values mean an increase in absorption, while negative −ΔT/T values represent an increase in transmission (bleach). In all cases we used 530 nm laser light excitation (160 Hz).

PTB7-Th(PCE10):PC70BM based solar cells

Table S5. Time zero photovoltaic device parameter for PTB7-Th:PC70BM based solar cells with and without $Ni(dtc)_2$ antioxidant.

Experiment	Jsc/mAcm^{-2} (SD)	Voc/V (SD)	FF (SD)	PCE (SD)
0wt%	15.6 (0.3)	0.809 (0.002)	0.64 (0.007)	8.1 (0.2)
4wt%	9.7 (0.4)	0.773 (0.02)	0.53 (0.05)	3.9 (0.5)

SD: standard deviation calculated from an average of 10 devices

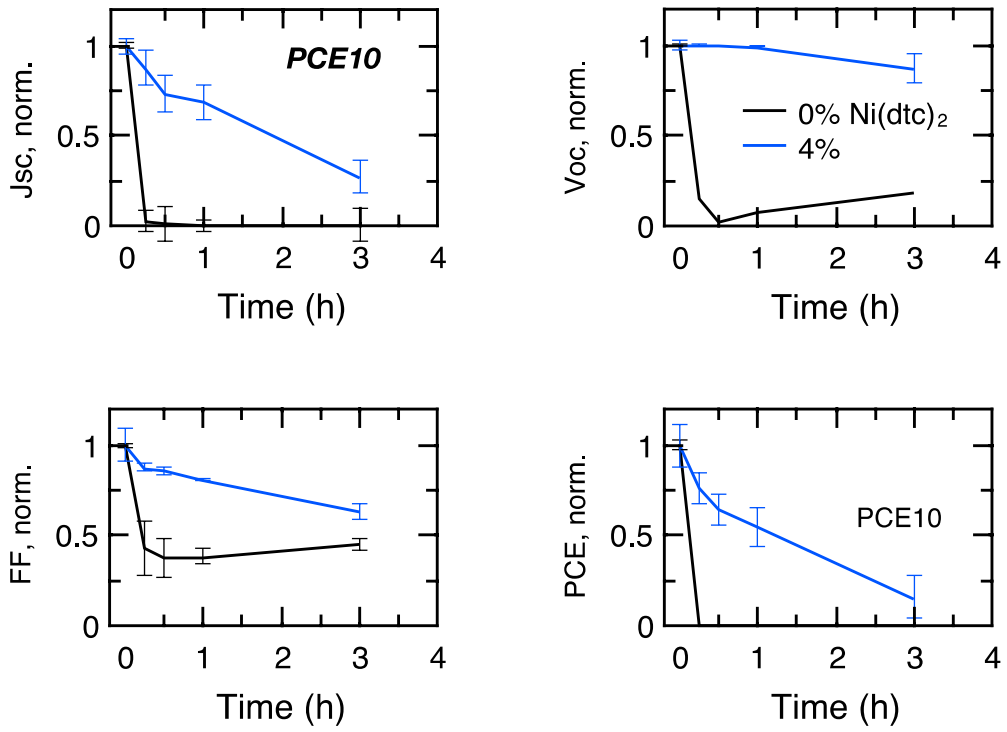

Figure S37. Photovoltaic parameters of PTB7-Th(PCE10):PC70BM half devices with and without $Ni(dtc)_2$ as a function of time of exposure to solar simulator light. Half devices were fabricated up to the active layer and completed with a MoOx/Ag top electrode after light exposure. A UV blocking filter (Lithoprotect yellow foil Y520E212) was employed to filter UV radiation from the solar simulator.

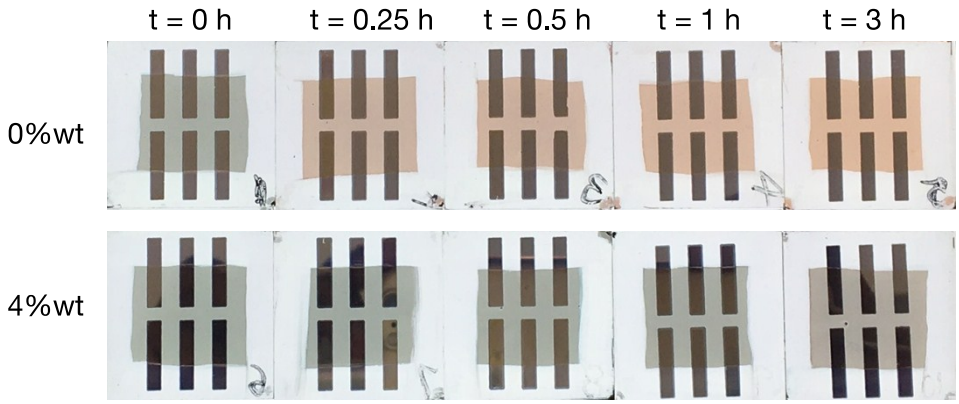

Figure S38. Photographs of photo-oxidized PTB7-Th-based devices upon different times of exposure. The devices are the same as the ones characterized in Figure S34.

PCPDTBT:PC70BM based solar cells

Table S6. Time zero photovoltaic device parameter for PCPDTBT:PC70BM based solar cells with and without $Ni(dtc)_2$ antioxidant.

Experiment	Jsc/mAcm^{-2} (SD)	Voc/V (SD)	FF (SD)	PCE (SD)
0wt%	8.4 (1.4)	0.544 (0.02)	0.30 (0.03)	1.5 (0.2)
2wt%	8.3 (0.3)	0.544 (0.002)	0.37 (0.01)	1.7 (0.1)

SD: standard deviation calculated from an average of 10 devices

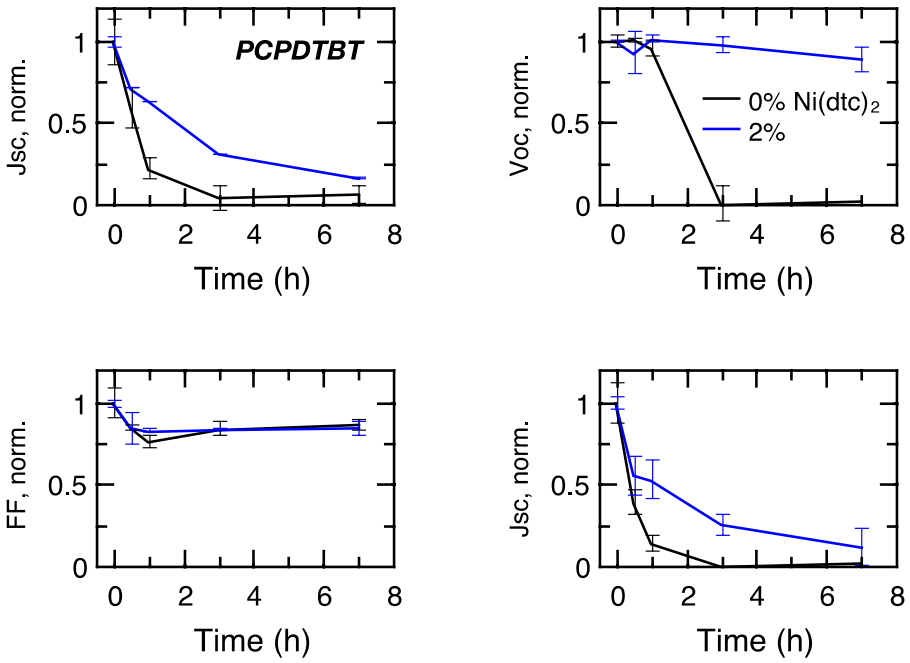

Figure S39. Photovoltaic parameters of PCPDTBT:PC70BM half devices with and without $Ni(dtc)_2$ as a function of time of exposure to solar simulator light. Half devices were fabricated up to the active layer and completed with a MoOx/Ag top electrode after light exposure. A UV blocking filter (Lithoprotect yellow foil Y520E212) was employed to filter UV radiation from the solar simulator.

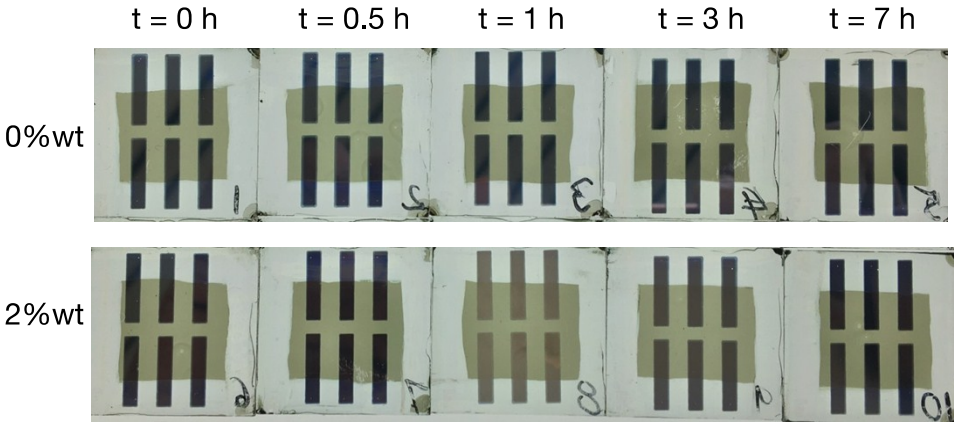

Figure S40. Photographs of photo-oxidized PCPDTBT-based devices upon different times of exposure. The devices are the same as the ones characterized in Figure S36.

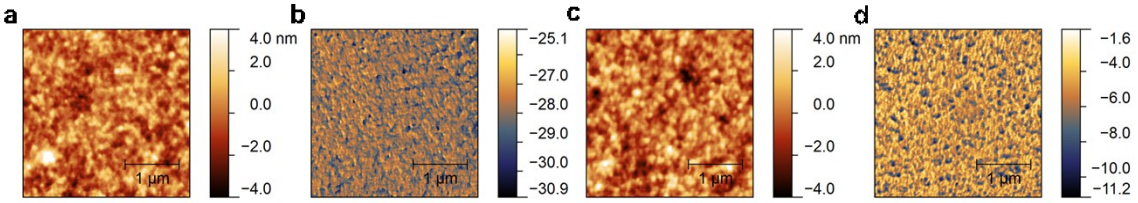

Figure S41. Intermittent contact atomic force micrographs of PCPDTBT:PCB70BM active layers with and without 4wt% of $Ni(dtc)_2$. **a**, topography of PCPDTBT:PCB70BM, **b**, AFM phase signal of PCPDTBT:PCB70BM, **c**, topography of PCPDTBT:PCB70BM:$Ni(dtc)_2$, **d**, AFM phase signal of PCPDTBT:PCB70BM:$Ni(dtc)_2$.

References

1. Basel, T. *et al.* Optical, Electrical, and Magnetic Studies of Organic Solar Cells Based on Low Bandgap Copolymer with Spin ½ Radical Additives. *Adv. Funct. Mater.* **25,** 1895–1902 (2015).
2. Soon, Y. W. *et al.* Correlating triplet yield, singlet oxygen generation and photochemical stability in polymer/fullerene blend films. *Chem. Commun.* **49,** 1291–1293 (2013).